

Fucosylated haptoglobin promotes inflammation via Mincle in sepsis: an observational study

Received: 5 June 2024

Accepted: 22 January 2025

Published online: 04 February 2025



Taylor Roh^{1,2,3,17}, Sungeun Ju^{4,17}, So Young Park^{5,17}✉, Yeonghwan Ahn⁴, Jiyun Chung⁴, Miyako Nakano⁶, Gyoungah Ryu^{1,2}, Young Jae Kim^{1,2,3}, Geumseo Kim^{1,2,3}, Hyewon Choi⁴, Sung-Gwon Lee⁷, In Soo Kim^{2,3,8}, Song-I Lee⁹, Chaeuk Chung¹⁰, Takashi Shimizu^{11,12}, Eiji Miyoshi¹³, Sung-Soo Jung¹⁴, Chungoo Park¹⁵, Sho Yamasaki^{11,12,16}, Seung-Yeol Park¹⁴✉ & Eun-Kyeong Jo^{1,2}✉

Haptoglobin (Hp) scavenges cell-free hemoglobin and correlates with the prognosis of human sepsis, a life-threatening systemic inflammatory condition. Despite extensive research on Hp glycosylation as a glyco-biomarker for cancers, understanding glycosylated modifications of Hp in sepsis patients (SPs) remains limited. Our study reveals elevated levels of terminal fucosylation at Asn207 and Asn211 of Hp in SP plasma, along with heightened inflammatory responses, compared to healthy controls (trial registration NCT05911711). Fucosylated (Fu)-Hp purified from SPs upregulates inflammatory cytokines and chemokines, along with NLRP3 inflammasome activation. Single-cell RNA sequencing identifies a distinct macrophage-like cell population with increased expressions of inflammatory mediators and *FUT4* in response to Fu-Hp. Additionally, Mincle, a C-type lectin receptor, interacts with Fu-Hp to amplify the inflammatory responses and signaling. Moreover, the Hp fucosylation (AAL) level significantly correlates with the levels of inflammatory cytokines in sepsis patients, suggesting that Fu-Hp is clinically relevant. Finally, Fu-Hp treatment significantly enhances the levels of inflammatory cytokines in the plasma and various tissues of mice. Together, our findings reveal a role of Fu-Hp, derived from sepsis patients, in driving inflammation, and suggest that targeting Fu-Hp could serve as a promising intervention for combating sepsis. Trial registration NCT05911711

Haptoglobin (Hp) is a prominent blood glycoprotein comprising α - and β -subunits. When bound to free hemoglobin (Hb), it forms a Hb-Hp complex, subsequently cleared by macrophages via the CD163 cell-surface receptor¹. This mechanism prevents tissue damage caused by free Hb and reduces iron loss in hemolytic conditions^{2,3}. Hp serves as a hub gene in sepsis, a persistent global health crisis^{4–7}, and is highly expressed during acute inflammatory responses and acute-phase

reactions⁸. Previous observational studies showed that elevated Hp levels correlate with reduced in-hospital mortality⁹ and improved outcomes¹⁰ in sepsis patients, suggesting a protective biomarker role beyond acute-phase reactivity. Glycosylation, a major post-translational modification, involves covalent linkage of carbohydrate chains to proteins, lipids, and nucleotides. Its significance in shaping structural and functional diversity is increasingly being recognized.

A full list of affiliations appears at the end of the paper. ✉ e-mail: sy.park12@gmail.com; seungpark@postech.ac.kr; hayoungj@cnu.ac.kr

Glycosylation patterns of various human plasma proteins significantly influence essential biological processes, including half-life in plasma, receptor interactions, and immune responses^{11–16}. Recent studies have explored the distinctive glycosylation status of Hp in various clinical conditions, especially in cancer^{2,10,17}. Core fucosylation (α 1-6 fucose) is increased in Hp from hepatocellular carcinoma¹⁸, whereas terminal fucosylation (α 1-3/4 fucose) is more closely associated with pancreatic, colon, and non-small cell lung cancers^{19–23}. Additionally, the glycan distribution is disease-specific. Among the four N-glycosylation sites (Asn184, Asn207, Asn211, and Asn241) in β -Hp, fucosylation increases at Asn241 in colon cancer^{21,22} and at Asn211 in pancreatic cancer^{19,20}. Also, β -Hp secreted in exosomes from cholangiocarcinoma exhibits a unique glycosylation profile and could serve as a diagnostic marker²⁴. The identification of cancer-specific Hp glycosylation in blood has attracted attention as a potential diagnostic biomarker for several human diseases^{17,20,25}. Nevertheless, the specific profiles and functions of Hp glycosylation in clinical conditions, particularly in life-threatening organ dysfunction associated with sepsis, remain unclear.

Macrophage-inducible C-type lectin (Mincle or CLEC4E), a receptor of the C-type lectin receptor (CLR) family, is predominantly expressed on myeloid cells and is important for initiating and modulating immune responses by recognizing pathogen glycolipids and lipid ligands from damaged cells^{26,27}. In sepsis, Mincle is implicated in both host defense and inflammatory injury. Mincle signaling is closely linked to tubular epithelial cell ferroptosis, thereby contributing to the development of sepsis-associated acute kidney injury²⁸. Nonetheless, Mincle deficiency impairs bacterial clearance and neutrophil function^{29,30}, underscoring its importance in maintaining immune balance in sepsis. Targeting Mincle could mitigate excessive inflammation and promote pathogen clearance, because dysregulated Mincle signaling may contribute to the pathogenesis of sepsis. Despite its importance, little is known about Mincle's function in the context of glycosylated proteins during sepsis, making this a crucial area for further investigation.

In this study, we investigate plasma Hp glycosylation in sepsis patients (SPs) compared to healthy controls (HCs), focusing on its impact on immune response regulation. SPs exhibit elevated terminal fucosylation at Asn207 and Asn211 of β -Hp. Isolated Fu-Hp from SPs induces inflammatory cytokines, chemokines, and NLRP3 inflammatory activation in human primary peripheral blood mononuclear cells (PBMCs) and monocytes. Importantly, Mincle is upregulated in SPs and interacted with Fu-Hp to induce an inflammatory response. Single-cell RNA sequencing (scRNA-seq) of Fu-Hp-treated PBMCs from HCs reveals a distinct macrophage-like cell subpopulation with elevated inflammatory mediators. We demonstrate the presence of an SP-specific macrophage-like cell population with Fu-Hp-associated gene signatures (*HP*, *FUT4*, *CLEC4E*, and *IL1B*), which was absent in non-surviving SPs. Finally, Fu-Hp treatment significantly increases the inflammatory cytokine levels in the plasma and various tissues of mice. These findings underscore the critical role of specific Hp glycosylation as a contributing factor of inflammatory responses in sepsis and highlight the potential for innovative interventions targeting the terminal fucosylation of Hp.

Results

Patient characteristics

The study population consisted of 152 patients with sepsis or septic shock from three centers (Chungnam National University Hospital [CNUH], Ewha Woman's Seoul Hospital, and Kangdong Sacred Heart Hospital) between 2018 and 2024. We defined sepsis as “life-threatening organ dysfunction caused by a dysregulated host response to infection,” and septic shock as “a subset of sepsis characterized by particularly profound circulatory, cellular, and metabolic abnormalities, clinically confirmed by the requirement of vasopressors to maintain a mean arterial pressure of 65 mm Hg or greater in the

absence of hypovolemia and a serum lactate level greater than 2 mmol/L (>18 mg/dL)”³¹. Initial assessment of patients with suspected sepsis involves basic laboratory tests, cultures, and imaging studies as deemed necessary, with evaluation of sepsis biomarkers such as procalcitonin and lactate levels. The demographic and laboratory characteristics of the patients are listed in Supplementary Data 1.

The most common cause was pneumonia, accounting for 85.7 % of the cases. Among the SPs, 73 (47.4 %) developed septic shock. Comorbidities were present in 124 SPs (81.5 %), with 45 patients having more than two comorbidities. Causative pathogens were identified in 87 SPs (57.2 %), with *Acinetobacter baumannii* being the most common pathogen in patients discharged from hospitals (8.6 %), while *Streptococcus pneumoniae* was the predominant pathogen in community-acquired pneumonia cases (5.2 %). Mechanical ventilators were used for 91 patients (59.1 %) and, among them, 27 (17.5 %) required a tracheostomy. The cornerstone of management is the rapid restoration of tissue perfusion and the early administration of antibiotics. Tissue perfusion is predominantly achieved by the aggressive administration of intravenous fluids (IVF), usually crystalloids at 30 mL/kg (actual body weight), started by 1 h and completed within 3 h following presentation. Vasopressor therapy is indicated if hypotension persists despite fluid administration.

SP survival was monitored for 28 days after ICU admission to assess the role of Hp. The 28-day mortality rate was 25.3 %. In multivariate analyses, age ($p = 0.027$, 1.06 [1.01–1.11]) and shock recovery status within 48 h ($p = 0.001$, 11.21 [3.49–36.03]) were independently correlated with the 28-day mortality rate.

Increased Hp fucosylation in SP plasma

To assess the glycosylation status in sepsis, various lectins were used to analyze the plasma samples collected from 121 SPs and 73 HCs (Supplementary Table 1). Blotting with *Aleuria aurantia* lectin (AAL) (against α 1-3/4/6 Fucose) revealed a markedly increased intensity in SPs ($n = 121$) compared to HCs ($n = 73$) (Fig. 1a). This change predominantly occurred around 45 kDa, possibly corresponding to β -Hp, as confirmed by reblotting for Hp (Supplementary Fig. 1a). There were no significant changes in the signals for other glycosyl epitopes between SPs and HCs (Supplementary Fig. 1b,c). These lectins included PHA-L (GlcNAc β 1-6Man α 1-6Man side chain; 121 SPs versus 73 HCs) and SNA (Neu5Ac α 2-3/6Glc/GalNAc; 121 SPs versus 73 HCs). To validate the observed increase in fucosylation attributed to β -Hp, Hp was purified from plasma using immunoaffinity chromatography and subjected to lectin blotting. AAL blotting showed that SP-Hp ($n = 20$) exhibited higher fucosylation levels compared to HC-Hp ($n = 20$) (Fig. 1b,c). This increase was attributed to additional fucose attachment rather than an increase in branched structures as there was no significant change in PHA-L blotting between the samples (Fig. 1b,c).

SP-Hp exhibited terminal fucosylated glycans at Asn207 and Asn211

To assess comprehensively the glycosylation status, we analyzed SP-Hp ($n = 6$) and HC-Hp ($n = 3$) using two independent approaches: a glycomic approach using LC(GC)-ESI MS and a glycoproteomic approach using LC(ODS)-ESI MS. Glycans can form antennary structures exhibiting bi-, tri-, and tetra-antennary branched configurations (Supplementary Fig. 1d). Fucose can be added to these structures, linked either through core fucosylation (α 1-6) or terminal fucosylation (α 1-3/4) (Supplementary Fig. 1d). LC(GC)-ESI MS analysis for desialo-glycans revealed that Hp from both cohorts exhibited similar proportions of antennary structures, with bi-antennary structures being the most prevalent, followed by tri- and tetra-antennary structures (Supplementary Fig. 1e–h). Notably, however, fucosylated glycan levels were significantly elevated in SP-Hp compared to HC-Hp (Fig. 1d, e). The increased fucosylation in SP-Hp resulted primarily from terminal fucosylation (α 1-3/4 fucose) rather than core fucosylation (α 1-6 fucose)

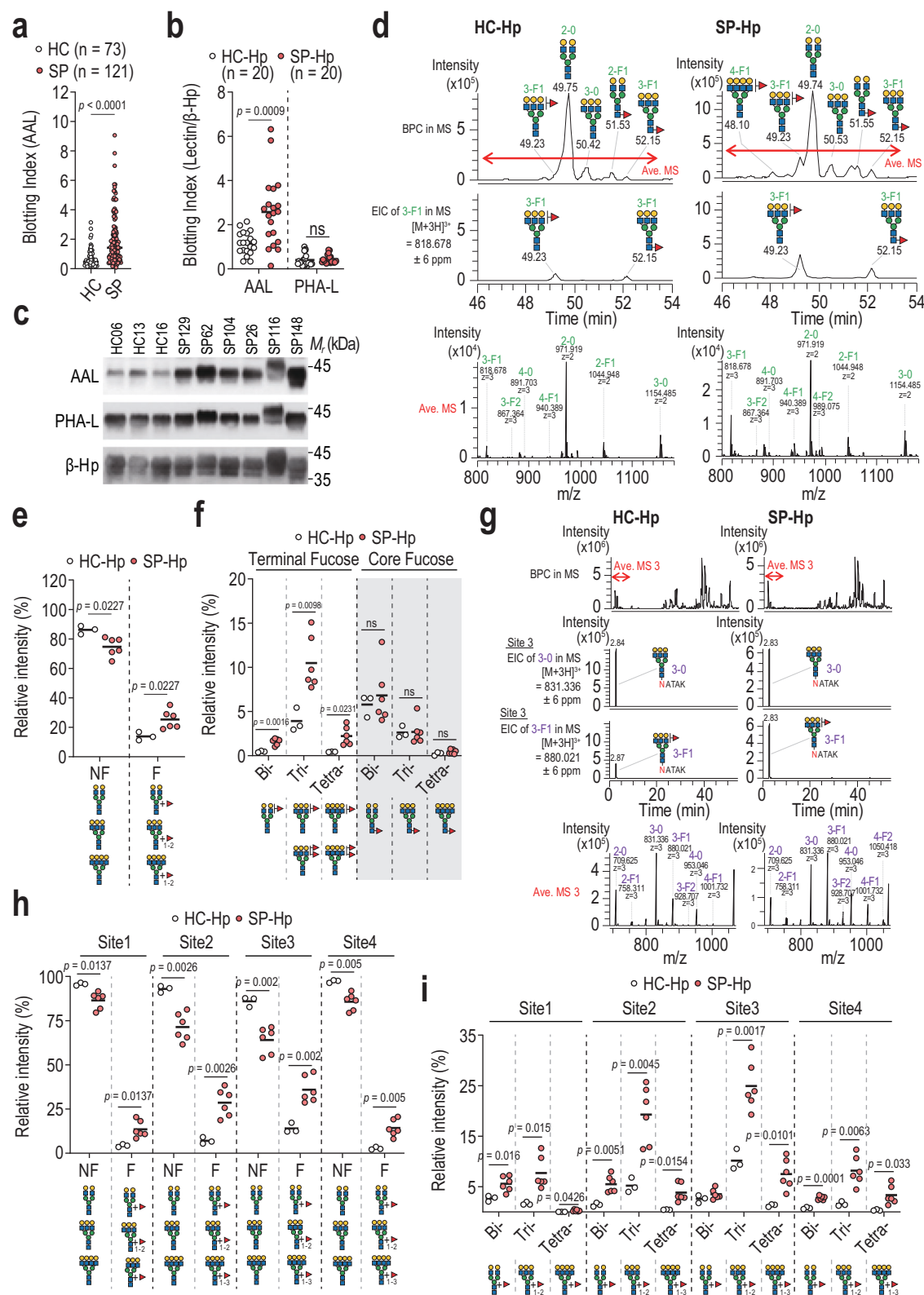


(Fig. 1d,f and Supplementary Fig. 1f). Among the three antennary structures, the increased terminal fucosylation in SP-Hp was predominantly attributed to tri-antennary structures (Fig. 1d,f and Supplementary Fig. 1f). A tetra-antennary structure with terminal fucosylation was detected at a low level in SP-Hp (Fig. 1f and Supplementary Fig. 1f).

To identify the glycosylation sites responsible for the increased fucosylation, site-specific analysis using LC(ODS)-ESI MS was

conducted (Fig. 1g and Supplementary Fig. 2a-d). Our findings revealed that glycans attached to Asn207 (Site 2) and Asn211 (Site 3) exhibited enhanced fucosylation in SP-Hp ($n = 6$) compared to HC-Hp ($n = 3$), while fucosylated glycans at these sites were reduced (Fig. 1h). Additionally, a marginal increase in fucosylation was observed at other glycosylation sites, including Asn184 (Site 1) and Asn241 (Site 4) (Fig. 1h). Among the antennary structures at Asn207 (Site 2) and Asn211 (Site 3) showing increased fucosylation, tri-antennary

Fig. 1 | Comparison of glycosylation status in Hp between SPs and HCs. **a** AAL blotting of the sera from sepsis patients ($n = 121$) and healthy donors ($n = 73$). Statistical significance was calculated with a two-sided unpaired t -test and presented as means \pm SD. **b,c** Lectin blotting for Hp purified from human sera with AAL and PHAL. The membrane was reblotting for β -Hp using anti-Hp antibody. Statistical significance was calculated with a two-sided unpaired t -test and presented as means \pm SD. **d** The top panels show base peak chromatogram (BPC) with structures of major N-glycans observed in this analysis using LC(GC)-ESI MS. The middle panels show extracted ion chromatogram (EIC) of mono-fucosylated tri-antennary N-glycan labeled with aTMT (m/z 818.678 \pm 6 ppm) of Hp samples (these are representative data for HC-Hp (HC2) and SP-Hp (SP32)). The bottom panels show average mass spectra (Ave. MS) during 46.0–53.0 min in BPC of the top panels. Structures, abbreviations and theoretical mass for N-glycans labeled with aTMT are shown in Supplementary Fig. 1d. **e** Relative abundances (%) of non-fucosylated and fucosylated N-glycans labeled with aTMT obtained from LC(GC)-ESI MS analyses of Hp samples ($n = 3$ for HC-Hp and $n = 6$ for SP-Hp). Statistical significance was calculated with a two-sided unpaired t -test and presented as means \pm SD. **f**, Relative abundances (%) of bi-, tri- and tetra-antennary N-glycans labeled with aTMT after

categorizing terminal- and core-fucosylation obtained from LC(GC)-ESI MS analyses of Hp samples ($n = 3$ for HC-Hp and $n = 6$ for SP-Hp). Statistical significance was calculated with a two-sided unpaired t -test and presented as means \pm SD. **g** The top panels show BPC of LC(ODS)-ESI MS analysis. The middle two panels show EIC of peptide (amino acid sequence is NATAK for site 3) containing non- and mono-fucosylated tri-antennary N-glycan (m/z 831.336 and 880.021 \pm 6 ppm for 3-O and 3-F1, respectively) of Hp samples (these are representative data for HC-Hp (HC2) and SP-Hp (SP32)). The bottom panels show average mass spectra (Ave. MS) during 2.6–3.3 min in BPC of the top panels. Structures, abbreviations and theoretical mass for desialo-glycopeptides on each site are shown in Supplementary Fig. 2a. **h** Relative abundances (%) of non-fucosylated and fucosylated N-glycans on glycopeptide at each site obtained from LC(ODS)-ESI MS analyses of Hp samples ($n = 3$ for HC-Hp and $n = 6$ for SP-Hp). Statistical significance was calculated with a two-sided unpaired t -test and presented as means \pm SD. **i**, Relative abundances (%) of bi-, tri- and tetra-antennary N-glycans on glycopeptide at each site obtained from LC(ODS)-ESI MS analyses of Hp samples ($n = 3$ for HC-Hp and $n = 6$ for SP-Hp). Statistical analysis was performed using the two-tailed Student's t -test (* $p < 0.05$; ** $p < 0.01$; *** $p < 0.001$; **** $p < 0.0001$). ns, not significant.

structures were the most fucose-abundant glycans in SP-Hp (Fig. 1i). The tetra-antennary structure was the most abundant and harbored fucose at Asn211; at Asn207, the biantennary structure was the next most abundant fucose-carrying structure (Fig. 1i). Altogether, our findings demonstrated that sepsis leads to increased terminal fucosylation in tri-antennary structures at Asn207 and Asn211 of plasma Hp.

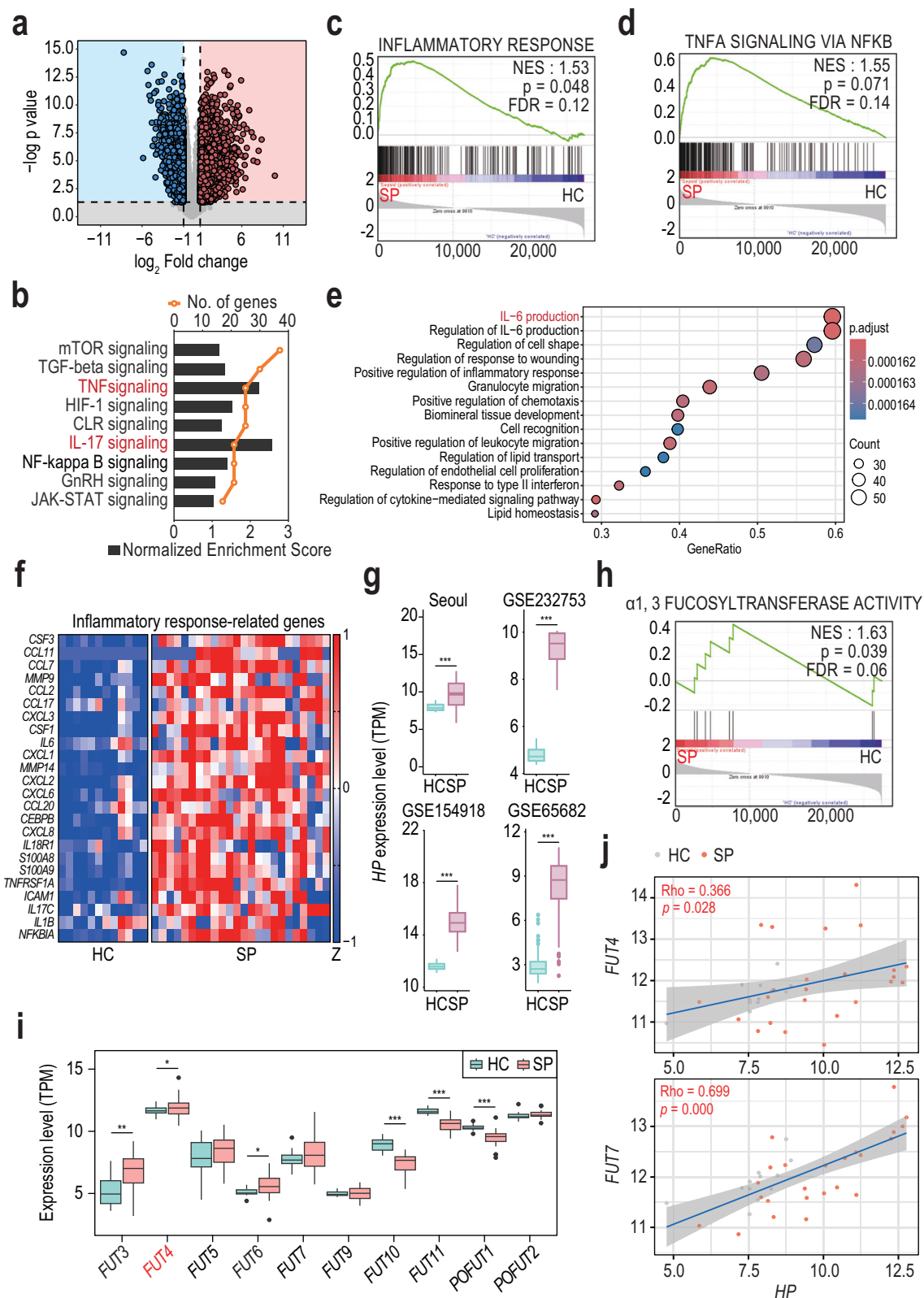
Transcriptomic analysis of PBMCs in HCs and SPs

Next, we investigated the transcriptomic differences in PBMCs between HCs ($n = 12$) and SPs ($n = 24$), termed the Seoul cohort, by bulk RNA sequencing (RNA-seq) analysis. Principal component analysis (PCA) of overall gene expression levels demonstrated a distinct separation between HCs and SPs, indicating significant differences in gene expression profiles within our Seoul cohort (Supplementary Fig. 3a,b). To identify the differentially expressed genes (DEGs) between HCs and SPs, we analyzed gene expression levels from the Seoul cohort datasets, revealing 6089 DEGs (2535 upregulated and 3554 downregulated) in PBMCs of SPs (Fig. 2a; DEGs are detailed in Supplementary Data 2). Based on these DEGs, we conducted gene set enrichment analysis using the KEGG, GO BP, and HALLMARK gene sets, revealing inflammation-related pathways as the most frequently enriched signaling pathways. Specifically, the DEGs were enriched in “IL-17 signaling”, “TNF signaling” (KEGG), “INFLAMMATORY RESPONSE”, “TNFA SIGNALING VIA NF κ B” (HALLMARK), and “IL-6 production” (GO BP) (Fig. 2b–e and Supplementary Fig. 3c). Heatmap data revealed elevated inflammation-related gene levels in SPs compared to HCs (Fig. 2f). Furthermore, *HP* expression was elevated in SPs of the Seoul cohort, as well as in three additional sepsis cohorts (GSE232753, GSE154918, and GSE65682) (Fig. 2g). Based on Hp fucosylation observed in SPs, we assessed the expression levels of genes related to fucosyltransferase activity using the “fucosyltransferase activity” gene set (GO:0046920). There was modest but significant upregulation of *FUT4* in SPs compared to HCs in the Seoul and GSE232753 cohorts (Fig. 2h,i and Supplementary Fig. 4). Other fucosyltransferase genes, such as *FUT10* and *FUT11*, were downregulated (Fig. 2i). The expression levels of fucosyltransferase genes, such as *FUT4* and *FUT7*, showed significant correlations with *HP* levels (Fig. 2j). These data suggest a role for *FUT4* in regulating terminal fucosylation of HP, which may influence its function during sepsis. Altogether, transcriptome analysis highlighted an intensified inflammatory response associated with elevated expressions of *HP* and several fucosyltransferases in PBMCs from SPs.

Fu-Hp induces inflammatory responses in human PBMCs

Based on the finding that SP increased terminal fucosylation of plasma Hp and augmented inflammatory responses in PBMCs, we evaluated the function of Fu-Hp on PBMCs. To this end, we treated PBMCs from HCs with purified HC-Hp isolated from the sera of healthy individuals (HC18 and HC25), and Fu-Hp isolated from the sera of two SP patients (SP41 and SP44). The PBMCs were incubated with HC-Hp or Fu-Hp for 6 h, followed by transcriptome analysis. A bulk RNA-seq analysis revealed a total of 1,290 DEGs (737 up-regulated and 553 down-regulated genes) in Fu-Hp-treated PBMCs compared to HC-Hp-treated PBMCs (Fig. 3a; DEGs are detailed in Supplementary Data 3). The significantly increased inflammatory cytokine/chemokine genes are labeled ($p < 0.05$; log₂(fold change) > 1 ; Fig. 3a). Gene set enrichment analysis utilizing KEGG gene sets revealed widespread distribution of DEGs across multiple signaling pathways associated with inflammatory responses, including NF- κ B signaling, TNF signaling, IL-17 signaling, chemokine signaling, and C-type lectin receptor signaling, in Fu-Hp-treated PBMCs (Fig. 3b). The heatmap highlighted significant disparities in the expression levels of inflammatory cytokines/chemokines between the two groups (Fig. 3c). Furthermore, an examination of DEGs using GO BP gene sets revealed activation of pathways, such as “Response to chemokine” (Fig. 3d).

Subsequently, we validated the mRNA expressions of the most common DEGs related to inflammatory cytokines and chemokines via qRT-PCR analysis in Fu-Hp-treated PBMCs relative to those treated with HC-Hp (Fig. 3e). Our findings revealed significant upregulation of mRNA and protein levels of proinflammatory cytokines and chemokines in PBMCs treated with Fu-Hp compared to those treated with HC-Hp (Fig. 3e,f). Western blotting analysis of the nuclear factor (NF)- κ B and mitogen-activated protein kinase (MAPK) signaling pathways demonstrated robust activation by Fu-Hp, similar to the response induced by lipopolysaccharide (LPS) stimulation, whereas HC-Hp did not elicit such activation (Fig. 3g). To investigate the potential variations in Fu-Hp among patients, Fu-Hp was extracted from SPs ($n = 20$). These samples significantly increased mRNA expression levels of *IL1B*, *IL6*, and *TNF* in human primary PBMCs compared to treatment with HC-Hp ($n = 20$) (Fig. 3h). Furthermore, the levels of inflammatory genes, *IL1B*, *IL6*, and *TNF*, correlated positively with AAL levels in both HCs and SPs (Fig. 3i). To determine whether these effects could be attributed to Hp fucosylation, HC PBMCs were treated with either non-glycosylated-Hp (NG-Hp) expressed in bacteria, or fucose alone. In the presence of LPS, *IL1B* and *TNF*



expression levels were significantly upregulated by Fu-Hp, whereas neither NG-Hp nor fucose alone induced such an increase (Fig. 3j and Supplementary Fig. 5). Collectively, these findings demonstrated the pivotal role of Fu-Hp from SPs in activating inflammatory signaling and responses in human immune cells.

Single-cell characterization of immune cells in Fu-Hp-treated PBMCs reveals a specific macrophage-like cluster associated with inflammatory responses

Next, we identified the immune cells implicated in Fu-Hp-induced inflammatory responses through scRNA-seq analysis. Human primary PBMCs from HCs ($n = 3$) were treated with or without Fu-Hp for 6 h.

Fig. 2 | Transcriptome profiling comparing PBMCs between SPs and HCs.

a Volcano plots showing DEGs between 24 SP and 12 HC in Seoul cohort. DEGs with significant ($p < 0.05$; $|\log_2(\text{fold change})| > 1$) changes were marked with colored dots. The blue dots represent the statistically significant downregulated genes, and the red dots represent the statistically significant upregulated genes. Statistical significance is observed for signatures above the dashed line. Two-sided p -values were calculated using the likelihood ratio test and adjusted for multiple comparisons using the Benjamini-Hochberg method to control the false discovery rate (FDR). **b** 9 inflammation-related KEGG pathways comparing PBMCs from SP and HC. The pathways that were significantly upregulated (q value < 0.05 ; normalized enrichment score > 2) were indicated as red color. Category names were shortened. Q values were calculated using the gseKEGG function of clusterProfiler package. **c, d** GSEA plot for inflammatory signatures comparing PBMCs from SP and HC. P values were determined by permutation test, and adjusted for multiple comparisons using the Benjamini-Hochberg method to control the false discovery rate (FDR). FDR < 0.25 ; NES, normalized enrichment score. **e** Dot plot showing the top 15 most significantly enriched GO biological process (BP) in PBMCs of SP vs HC; color indicates adjusted p values, while the dot size represents the gene count associated with each pathway. The p values were calculated using the hypergeometric test and adjusted for multiple comparisons using the two-sided Benjamini-Hochberg method. **f** Heatmap depicting TPM values of inflammatory response-related genes from IL-17 signaling, TNF signaling (KEGG) and Inflammatory response (HALLMARK) geneset

in PBMCs of SP ($n = 24$) versus HC ($n = 12$). Z-score (Z). **g** Box-and-whisker plot illustrating the expression of the *HP* gene across four cohorts: Seoul, GSE232753, GSE154918, and GSE65682. The lower and upper hinges of the box represent the 25th and 75th percentiles, and the whiskers extend to the minimum and maximum values within 1.5 times the interquartile range. The median value is depicted by the line within the box. Statistical significance was calculated with a two-tailed t -test without adjustment ($***p < 0.001$). **h** GSEA plot for ‘ α 1,3 FUCOSYLTRANSFERASE ACTIVITY’ GO molecular function (MF) gene set in PBMCs of SP vs HC. P values were determined by permutation test, and adjusted for multiple comparisons using the Benjamini-Hochberg method to control the false discovery rate (FDR). **i**, Box-and-whisker plot illustrating the expression of the indicated genes. The lower and upper hinges of the box represent the 25th and 75th percentiles, and the whiskers extend to the minimum and maximum values within 1.5 times the interquartile range. The median value is depicted by the line within the box. Statistical significance was calculated with a two-tailed t -test without adjustment ($*p < 0.05$; $**p < 0.01$; $***p < 0.001$). **j** Correlation between the expression of the *HP* gene (x-axis) and the expression of either the *FUT4* or *FUT7* gene (y-axis) with the best linear fit plotted. Pearson correlation coefficients were calculated to assess the linear association. The shaded area represents the 95 % confidence interval. P values were calculated using a t -distribution with $[n-2]$ degrees of freedom. Pearson's correlation coefficient and the p value are displayed in the top-left corner.

From these, a total of 31,024 filtered cells with at least 500 and fewer than 5000 detected genes and below 25 % mitochondrial transcripts were selected for further analysis, yielding an average of approximately 4974 mapped reads and 2000 genes per cell. As expected, an unbiased clustering analysis revealed distinct PBMC clusters (Fig. 4a,b), encompassing various immune cell types, including macrophage-like cells (MLCs; *IL12B* and *CCL15*), monocytes (*CST3* and *CD14*), natural killer (NK) cells (*FCGR3A*), B cells (*CD79A*), CD4 + T cells (*CD4* and *SELL*), and CD8 + T cells (*CD8*) (Supplementary Fig. 6a). There was a significant decrease in the percentage of monocytes, while the heterogeneity of macrophage-like subclusters expanded considerably following Fu-Hp treatment (Fig. 4b,c). Within these macrophage-like subclusters, the expression of genes associated with inflammation exhibited a significant increase ($\log_2(\text{fold change}) > 1$, $p < 0.05$; Fig. 4d). Since the macrophage-like compartment underwent the most pronounced alteration in response to Fu-Hp, we conducted an unsupervised cluster analysis to investigate the heterogeneity and function of macrophage-like subpopulations (Fig. 4e,f, and Supplementary Fig. 6b), and three macrophage-like subclusters (7, 18, and 29) were identified (Fig. 4a). Macrophage-like cluster 7 (MLC-7) exhibited relatively high expression levels of antigen-presentation genes, including *LILRB2*, *LILRA5*, *CD74*, and *HLA-DRA*, characteristics akin to the previously reported major antigen-presenting macrophage cluster³². MLC-18 was marked by the expression of proinflammatory genes, including *IL1A*, *CXCL1*, *CXCL2*, *CXCL3*, *CXCL5*, and *CXCL8*, resembling the signatures of M1-like macrophages (Fig. 4e,f). MLC-29 showed enrichment in *MALAT1*, *SYNE2*, and *PDE3B* (Fig. 4f and Supplementary Data 4). Among these macrophage-like subclusters (MLC-7, -18, and -29), MLC-18 exhibited the highest expression of cytokines and chemokines (Fig. 4e,f, and Supplementary Data 4).

Consistent with the observation in PBMCs, the mRNA levels of proinflammatory cytokines/chemokines exhibited a significant elevation in human primary monocytes following Fu-Hp treatment, compared to those treated with HC-Hp (Fig. 5a). Notably, *Il1b*, *Il6*, and *Tnf* were also elevated in mouse bone marrow-derived macrophages (BMDMs; Fig. 5b). Furthermore, Fu-Hp treatment significantly enhanced the secretion levels of IL-1 β , IL-6, and TNF in both human monocytes (Fig. 5c) and mouse BMDMs (Fig. 5d). Similarly, Fu-Hp treatment of mouse macrophage RAW264.7 cells led to an increase in mRNA expression levels of various proinflammatory cytokines and chemokines (*Tnf*, *Il1b*, *Il6*, *Ccl2*, *Ccl3*, and *Ccl4*), without affecting *Il10* expression (Fig. 5e). Consistent with the findings observed in PBMCs

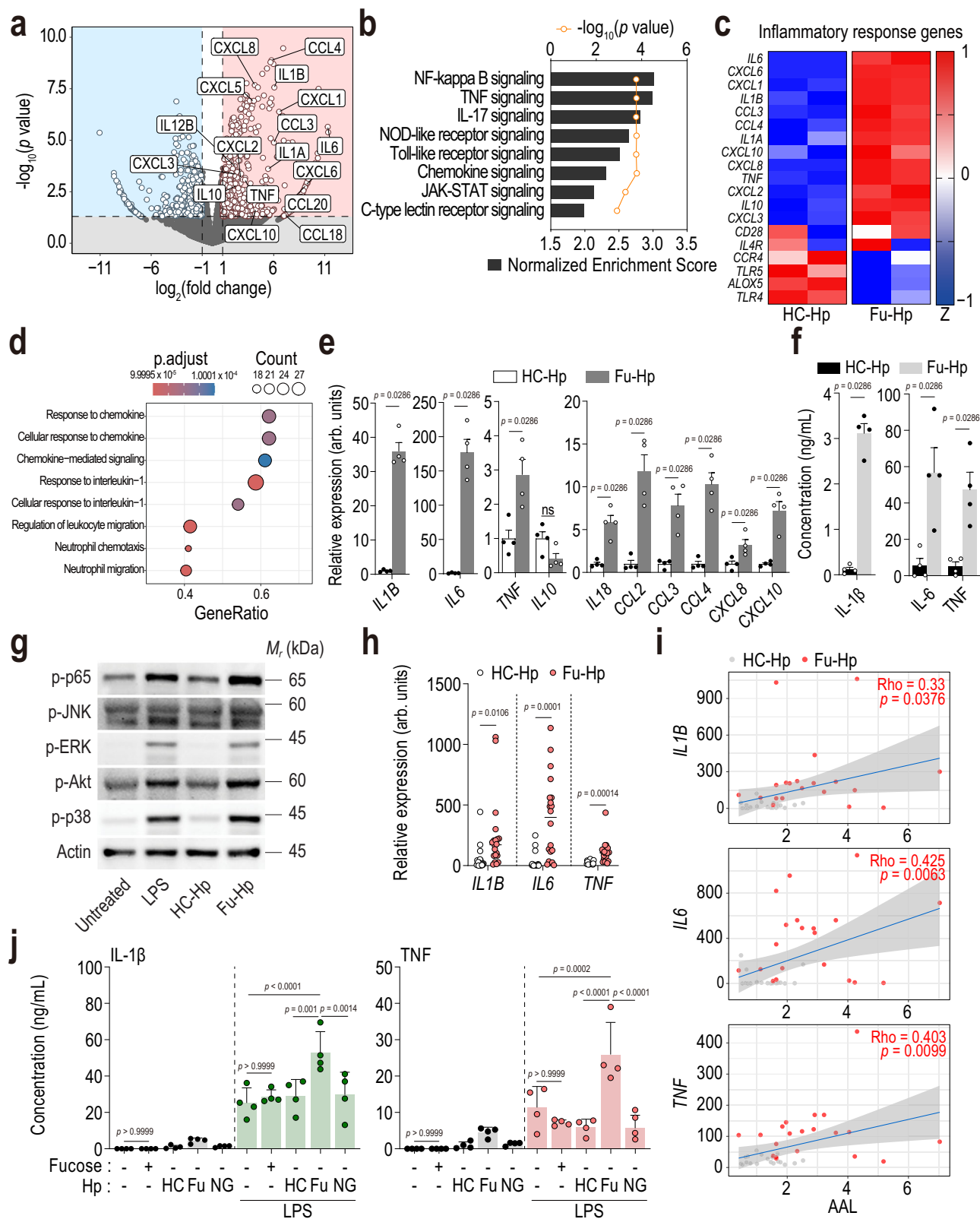
(Fig. 3g), Fu-Hp treatment induced activation of the NF- κ B and MAPK pathways in both human monocytes and mouse BMDMs (Fig. 5f,g, and Supplementary Fig. 7a,b). Together, these results suggest that Fu-Hp induces distinct macrophage-like subsets from healthy PBMCs.

Fu-Hp from SPs enhanced NLRP3 inflammasome activation in human monocytes

Given the pivotal role of the NLRP3 inflammasome in sepsis, we further investigated the impact of Fu-Hp on its regulation. Various Fu-Hp samples from SPs, but not Hp samples from HCs, induced the maturation of pro-IL-1 β and pro-caspase-1 into IL-1 β and caspase-1, respectively, in human primary monocytes, regardless of LPS priming (Fig. 5h). Furthermore, silencing NLRP3 in human monocytes resulted in a significant reduction in IL-1 β secretion in LPS-primed, Fu-Hp-stimulated monocytes (Fig. 5i). As a control, TNF secretion remained unaffected by NLRP3 silencing in human primary monocytes stimulated with Fu-Hp (Fig. 5i). Mechanistically, Fu-Hp significantly increased mitochondrial reactive oxygen species (mtROS) generation in human primary monocytes (Supplementary Fig. 8a). Conversely, pretreatment with mitoTEMPO, a mtROS scavenger, alleviated the induction of mtROS generation by Fu-Hp (Supplementary Fig. 8a). Treatment of mitoTEMPO, but not K⁺ efflux, significantly inhibited the Fu-Hp-induced secretion of IL-1 β in human primary monocytes (Fig. 5j,k) and PMA-differentiated THP-1 cells (Supplementary Fig. 8b,c). Collectively, these findings suggest that Fu-Hp activates the NLRP3 inflammasome complex in human monocytes through mtROS release.

Fu-Hp induces and interacts with CLEC4E/Mincle receptor

To identify the key innate immune gene(s) associated with Fu-Hp, we analyzed DEGs from three SP cohorts (Seoul, GSE232753, and GSE65682), scRNA-seq data (Fig. 4a-d), and the ‘‘Innate immune response’’ GO gene set (Fig. 6a). Transcriptomic analysis of the Seoul RNA-seq cohort revealed 4,330 significantly upregulated genes in SPs compared to HCs ($p < 0.05$; \log_2 fold change > 0), with 236 of these genes associated with innate immunity (Fig. 6a; Supplementary Data 2). Similarly, the GSE232753 RNA-seq cohort demonstrated upregulation of 4,648 genes in SPs ($p < 0.05$; \log_2 fold change > 0), including 291 related to innate immunity (Fig. 6a). The GSE65682 microarray cohort exhibited upregulation of 99 genes in SPs ($p < 0.05$; \log_2 fold change > 0), with 24 genes involved in innate immunity (Fig. 6a). Moreover, the scRNA data of Fu-Hp treated PBMCs revealed



67 upregulated genes ($p < 0.05$; \log_2 fold change > 0) in the macrophage-like cell population of Fu-Hp treated PBMCs, with 11 genes related to the innate immune response (Fig. 6a). This analysis allowed identification of *CLEC4E* upregulation, which was consistent across multiple datasets (Fig. 6b) and within the innate immune response pathway. *CLEC4E* expression was also significantly elevated in macrophages-like subclusters (Fig. 6c), specifically in the MLC-18

cluster (Fig. 6d) of scRNA-seq data from Fu-Hp-treated PBMCs. *CLEC4E* was upregulated in the Fu-Hp-treated compared to HC-Hp-treated PBMCs (Supplementary Data 3).

We investigated the impact of Fu-Hp treatment on *CLEC4E* gene expression in human primary monocytes using quantitative real-time polymerase chain reaction. At each time-point examined, Fu-Hp-treated cells exhibited elevated *CLEC4E* gene expression levels

Fig. 3 | Fu-Hp induces inflammatory responses in human primary PBMCs. **a** Volcano plots showing DEGs in PBMCs after Fu-Hp ($n = 2$) or HC-Hp ($n = 2$) treatment (20 $\mu\text{g}/\text{mL}$ for 6 h). DEGs with significant ($p < 0.05$; $|\log_2(\text{fold change})| > 1$) changes were marked with colored dots. Significantly increased cytokine/chemokine genes were labeled. Statistical significance is observed for signatures above the dashed line. Two-sided p -values were calculated using the likelihood ratio test and adjusted for multiple comparisons using the Benjamini-Hochberg method to control the false discovery rate (FDR). **b** Top 8 inflammation-related KEGG pathways comparing Fu-Hp-treated PBMCs and HC-Hp-treated PBMCs. Category names were shortened. P values were calculated using the cumulative hypergeometric distribution. **c** Heatmap depicting TPM values of inflammatory response genes (HALLMARK) in HC-Hp or Fu-Hp-treated PBMCs. Z-score (Z). **d** Dot plot depicting the eight most significantly enriched GO BP, comparing PBMCs treated with Fu-Hp to untreated controls. Color indicates adjusted p values, while the dot size represents the gene count associated with each pathway. The p values were calculated using the hypergeometric test and adjusted for multiple comparisons using the two-sided Benjamini-Hochberg method. **e** The relative expression of inflammatory genes, including *IL1B*, *IL6*, *TNF*, *IL10*, *IL18*, *CCL2*, *CCL3*, *CCL4*, *CXCL8*, and *CXCL10* in PBMCs after treatment with HC-Hp or Fu-Hp using qRT-PCR ($n = 4$ per group). Statistical significance was calculated with a two-sided unpaired t -test with Mann-

Whitney test and presented as means \pm SEM. arb. units, arbitrary unit; ns, not significant. **f**, The concentrations of IL-1 β , IL-6, and TNF in the supernatants of HC-Hp or Fu-Hp treated-PBMCs (20 $\mu\text{g}/\text{mL}$ for 18 h) measured by ELISA ($n = 4$ per group). Statistical significance was calculated with an unpaired t -test with Mann-Whitney test and presented as means \pm SEM. **g** Western blotting for phosphorylated NF- κB (p-p65), phosphorylated ERK (p-ERK), phosphorylated JNK (p-JNK), phosphorylated Akt (p-Akt), and phosphorylated p38 (p-p38) in HC-Hp or Fu-Hp-treated PBMCs ($n = 1$; 20 $\mu\text{g}/\text{mL}$ for 30 min). **h** The relative expression of *IL1B*, *IL6*, and *TNF* in PBMCs from a healthy donor after treatment with HC-Hp or Fu-Hp derived from different 20 people (20 $\mu\text{g}/\text{mL}$ for 6 h) using qRT-PCR. Statistical significance was calculated with a two-tailed unpaired t -test and presented as means \pm SD. arb. units, arbitrary unit. **i**, Correlation between the expression of the AAL level (x-axis) and the expression of either the relative expression of indicated genes (*IL1B*, *IL6*, and *TNF*) (y-axis) with the best linear fit plotted ($n = 20$ per each group). The shaded area represents the 95 % confidence interval. P values were calculated using a t -distribution with $[n-2]$ degrees of freedom. Pearson's correlation coefficient and the p value are displayed in the top-right corner. **j** The concentrations of IL-1 β and TNF in the supernatants of PBMCs measured by ELISA ($n = 4$ per group). PBMCs were treated L-fucose and Hp. Statistical significance was calculated with a one-way ANOVA test with Bonferroni's multiple correction and presented as means \pm SEM.

compared to those treated with HC-Hp (Fig. 6e). We next questioned whether *CLEC4E*-encoding Mincle physically interacts with Fu-Hp. To investigate the interaction between Mincle and Hp, we incubated immunoprecipitated HA-Mincle with purified Hp (isolated from the plasma of SP50) and found that Fu-Hp interacted with Mincle (Fig. 6f). The interaction was diminished when the fucosylation of SP-Hp was removed by fucosidase pre-treatment (Fig. 6f). As depicted in Fig. 6g, we further conducted immunoprecipitation using four distinct Hp samples (SP48, SP57, SP59, and SP60) per group. Quantitative graph revealed that Fu-Hp exhibited a significantly higher binding affinity to Mincle compared to HC-Hp, and this interaction was markedly inhibited by fucosidase. To validate this interaction at the cell membrane, we expressed SNAP-Mincle in cells and incubated them with ATTO 488 dye-labeled Hp. Total internal reflection fluorescence (TIRF) microscopy revealed a higher degree of colocalization between Mincle and SP-Hp, compared to HC-Hp (Fig. 6h-j). Furthermore, we measured the affinity between Mincle and Fu-Hp by microscale thermophoresis (MST). Mincle showed higher affinity to Fu-Hp ($\text{KD } 5.7 \pm 1.01 \mu\text{M}$) than HC-Hp ($\text{KD } 22.9 \pm 5.15 \mu\text{M}$) (Fig. 6k,l). These results suggest that Fu-Hp induces the expression of and interacts with Mincle receptor.

The interaction between Fu-Hp and *CLEC4E*/Mincle receptor triggers inflammatory signaling and responses

We examined whether the Fu-Hp/Mincle interaction leads to the activation of inflammatory responses in monocytes/macrophages. Knockdown of *CLEC4E* significantly reduced the expression of *IL1B* and *IL6* induced by Fu-Hp (Fig. 7a). Blocking the Mincle pathway using anti-human Mincle neutralizing antibodies (NM) also inhibited the secretion of mature IL-1 β and mature caspase-1 by human primary monocytes (Fig. 7b,c). To validate these findings, we used a *Clec4e* knockout (KO) mouse line to assess the inflammatory activity of Fu-Hp in BMDMs. The Fu-Hp-induced expression levels of *Il1b* and *Il6* were significantly downregulated in *Clec4e*^{KO} BMDMs compared to *Clec4e*^{WT} BMDMs (Fig. 7d). Consistently, the secretion of IL-1 β and IL-6 induced by Fu-Hp, as well as the expression of pro-IL-1 β , pro-caspase-1, and IL-6, were significantly reduced in *Clec4e*^{KO} BMDMs compared to *Clec4e*^{WT} BMDMs (Fig. 7e,f).

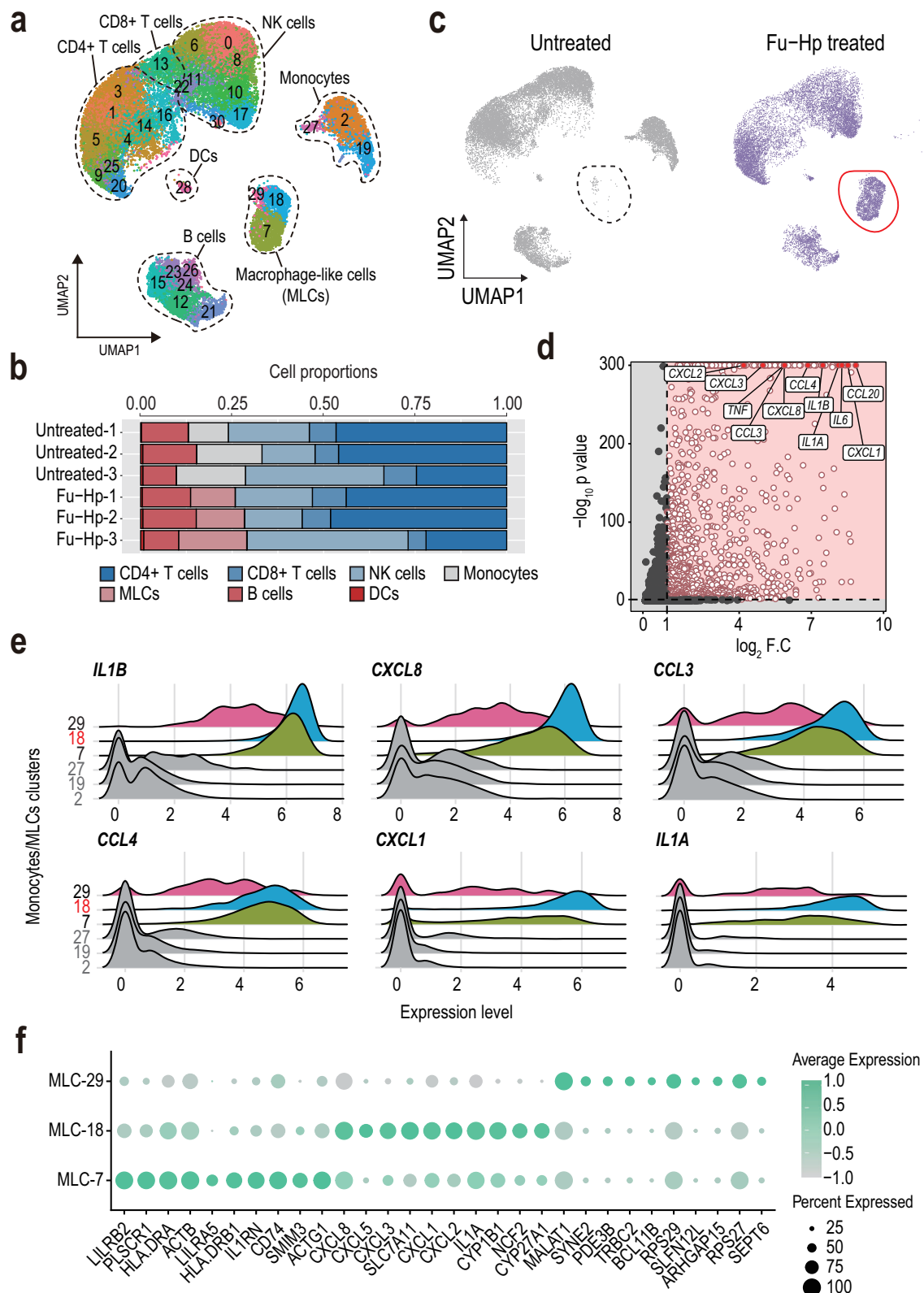
The activation of nuclear factor of activated T cells (NFAT) is crucial for evaluating the biological activity of Mincle agonists^{33,34}. The interaction between Mincle and α -mannosyl residues on fungi triggers activation of NFAT reporter genes, leading to enhanced inflammatory responses³⁴. Therefore, we examined whether samples of Fu-Hp (SP65, SP69, SP70, and SP82) would induce NFAT activation by luciferase

assay in HeLa cells co-transfected with *CLEC4E* and NFAT reporter constructs (Fig. 7g). As shown in the figure, the four Fu-Hp samples significantly increased NFAT transcriptional activity compared to the four HC-Hp samples (HC23, HC26, HC31, and HC32). As a positive control, trehalose 6,6'-dimycolate (TDM) from *Mycobacterium tuberculosis* enhanced NFAT transcriptional activity in Mincle-transfected HeLa cells similar to that induced by Fu-Hp. These results suggest that the Fu-Hp-Mincle interaction induces inflammatory responses and NFAT signaling in monocytes/macrophages.

Macrophage populations with Fu-Hp-associated gene signatures disappear in non-surviving SPs

To understand the clinical relevance of Fu-Hp in sepsis prognosis, we conducted scRNA-seq analysis on PBMCs from two distinct groups of SPs, categorized as survivors (S-SP; SP30) and non-survivors (NS-SP; SP29), as well as two HCs. Consensus-based assignment of cell types across all participants revealed seven distinct cell types: CD4 + T cells (37 %), CD8 + T cells (4 %), B cells (12 %), NK cells (21 %), monocytes (10 %), MLC-NS (8 %), and MLC-S (7 %) (Fig. 8a). Consistent with previous findings following Fu-Hp administration in PBMCs from HCs (Fig. 4), we observed an increase in MLC populations in SPs, compared to HCs (Fig. 8b). In HCs, approximately 17.1 % of the cells were identified as monocytes, with MLCs constituting approximately 0.89 %. In SPs, the proportion of monocytes decreased to around 0.73 %, with MLCs constituting approximately 36.5 % (Fig. 8a). Furthermore, these MLCs were subdivided into two clusters (MLC-S and -NS) based on patient survival outcomes (Fig. 8a and Supplementary Data 1). In S-SP sample, MLC-NS accounted for less than 1 % of the population, while MLC-S comprised 33.2 %. Conversely, in NS-SP samples, the frequency of MLC-NS was significantly higher at around 39.7 %, with MLC-S being scarcely detected (Fig. 8c). MLC-S from S-SPs exhibited increased expression of *HP*, *FUT4*, *CLEC4E*, and *IL1B*, whereas these genes were expressed at lower levels in MLC-NS from NS-SPs (Fig. 8d). The expression levels of cytokine/chemokine-related genes (*CXCL8* and *CCL3*) were not significantly increased in MLC-S, whereas those of *CXCL2* and *CXCL3* decreased in MLC-S compared to MLC-NS (Fig. 8d and Supplementary Data 5).

To validate our findings, we conducted an analysis using the publicly available data of a cohort of sepsis patients (GSE167363; Fig. 8e-g and Supplementary Fig. 9). There was a notable increase in a specific cell population (cluster 3) among S-SPs ($n = 6$) but not among NS-SPs ($n = 4$) (Fig. 8e-g). In cluster 3, the levels of *HP*, *FUT4*, *CLEC4E*, and *IL1B*, along with macrophage markers (*CD14*, *ITGAM*, and *FCGR3A*),



were increased compared to other clusters (Fig. 8h). Furthermore, in the Seoul cohort, we found significant upregulation of *FUT4*, *CLEC4E*, and *IL1B* among S-SPs compare to HCs with a more pronounced increase observed than in NS-SPs (Fig. 8i). These findings support the association between Fu-Hp-associated gene signatures and favorable outcomes in sepsis.

We then assessed the correlations between Fu-Hp levels, immune profiles, and clinical data in S-SPs, NS-SPs, and HCs. In the Seoul cohort, we observed elevated *IL1B* and *IL6* levels in S-SPs ($n = 19$), contrasting with the diminished expression in NS-SPs ($n = 5$; Fig. 8j), indicating immunosuppression in NS-SPs. Notably, *IL1B* and *IL6* levels strongly correlated with Hp fucosylation (AAL) in all participants

Fig. 4 | ScRNA-seq analysis of Fu-Hp-treated PBMCs reveals a distinct macrophage-like cell cluster associated with inflammatory responses.

a Unsupervised UMAP analysis on PBMCs pooled from three untreated and three Fu-Hp treated persons (16961 cells untreated, 14063 cells Fu-treated). Cell populations were mapped onto the UMAP landscape to visualize the distribution of cells across clusters using the RunUMAP and Dimplot function in Seurat package. **b** Bar plot of the proportion of cell types shown in **a**, separated by 3 untreated samples and 3 Fu-Hp-treated samples. **c** The UMAP plot illustrating the alterations in cell

proportions induced by Fu-Hp treatment. **d** Volcano plot depicting increased DEGs in Fu-Hp-treated PBMCs. Significantly increased cytokine/chemokine genes were labeled (adjusted p values $< 0.06^{<301}$). P values were calculated by the FindMarkers function in Seurat 5.0.1 package using the default two-sided Wilcoxon Rank Sum test. **e** Ridge plots displaying the expression patterns of indicated genes in subpopulations of monocytes (2, 19, and 27) and macrophages (7, 18, and 29). **f** Expression of selected markers for sub-clusters (7, 18, and 29) of MLC populations.

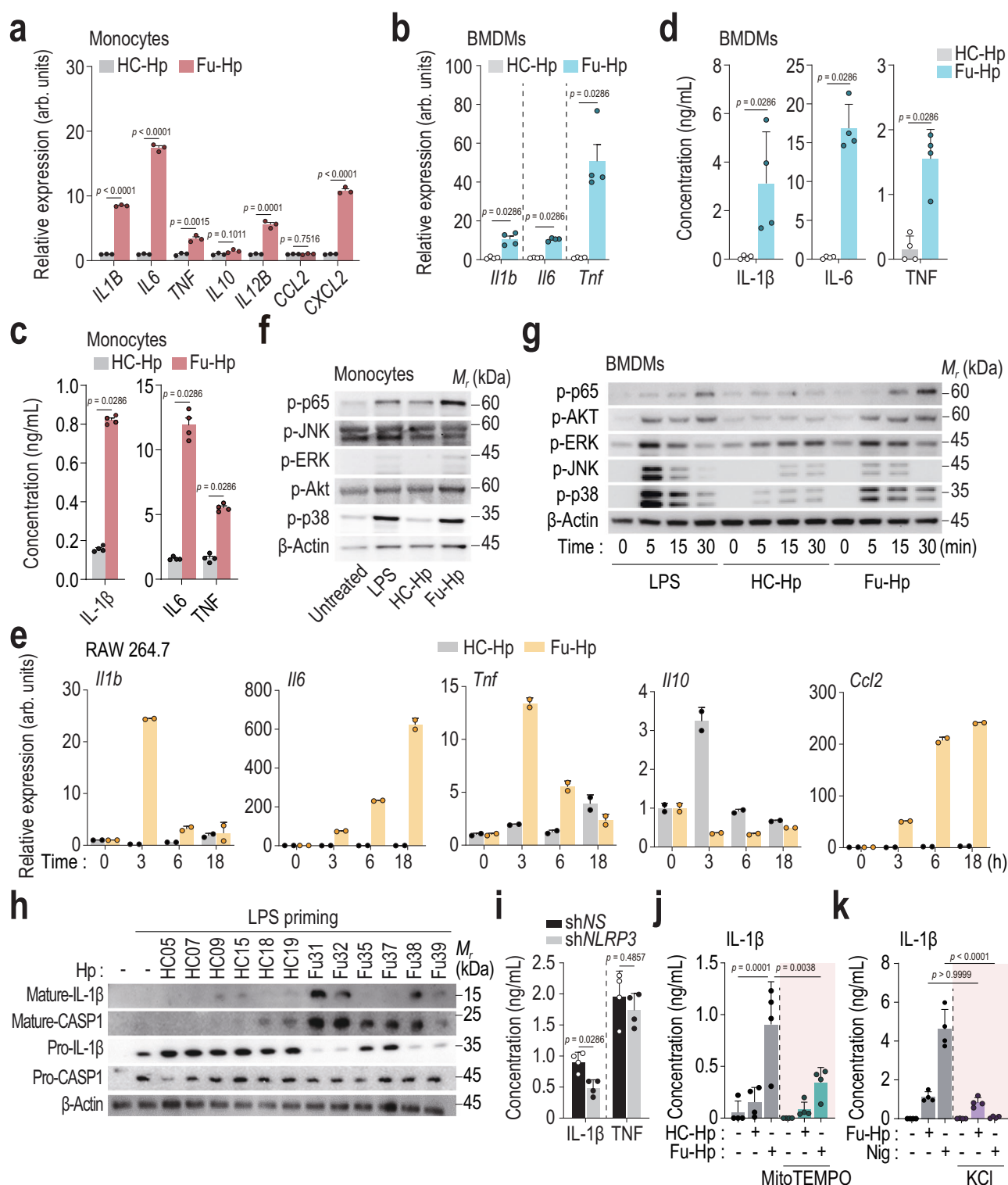


Fig. 5 | Fu-Hp induces inflammatory responses and NLRP3 inflammasome activation in monocytes and macrophages. **a** The relative expression of *IL1B*, *IL6*, *TNF*, *IL10*, *IL12B*, *CCL2*, and *CXCL2* in monocytes from a HC after treatment with HC-Hp or Fu-Hp (20 µg/mL for 6 h) using qRT-PCR ($n = 3$ per each group). Statistical significance was calculated with a two-tailed unpaired *t*-test and presented as means \pm SD. arb. units, arbitrary unit. ns, not significant. **b**, The relative expression of *Il1b*, *Il6*, and *Tnf* in mouse BMDMs after treatment with HC-Hp or Fu-Hp (100 µg/mL for 6 h) using qRT-PCR ($n = 4$ per each group). Statistical significance was calculated with an unpaired *t*-test with Mann-Whitney test and presented as means \pm SEM. arb. units, arbitrary unit. **c,d** The concentrations of IL-1 β , IL-6, and TNF in the supernatants of HC-Hp or Fu-Hp-treated cells measured by ELISA ($n = 4$ per group). Statistical significance was calculated with an unpaired *t*-test with Mann-Whitney test and presented as means \pm SEM. **e**, The relative expression of *Il1b*, *Il6*, *Tnf*, *Il10*, and *Ccl2* in RAW264.7 cells after treatment with HC-Hp or Fu-Hp (20 µg/mL for 6 h) using qRT-PCR ($n = 2$ per each group). **f,g** Western blotting for phosphorylated NF- κ B (p-p65), phosphorylated ERK (p-ERK), phosphorylated JNK (p-JNK),

phosphorylated Akt (p-Akt), and phosphorylated p38 (p-p38) in human primary monocytes (**f**) or mouse BMDMs (**g**). **h** Western blotting for mature IL-1 β , mature caspase1, pro-IL-1 β , and pro-caspase1 in human primary monocytes treated for 18 h with Fu-Hp after LPS priming. **i** The concentrations of IL-1 β and TNF in the supernatants of human primary monocytes with Fu-Hp treatment after shNS or shNLRP3 virus knockdown measured by ELISA ($n = 4$ per group). Statistical significance was calculated with a two-sided unpaired *t*-test with Mann-Whitney test and presented as means \pm SD. **j** The concentrations of IL-1 β in the supernatants of human primary monocytes with Fu-Hp treatment after mitoTEMPO pre-treatment or not measured by ELISA ($n = 4$ per group). Statistical significance was calculated with a one-way ANOVA with Bonferroni test and presented as means \pm SD. **k** The concentrations of IL-1 β in the supernatants of human primary monocytes with Fu-Hp treatment after potassium chloride (KCl) pre-treatment or not measured by ELISA ($n = 4$ per group). Statistical significance was calculated with a one-way ANOVA with Bonferroni test and presented as means \pm SD.

($R = 0.49$ and $= 0.36$, $p = 0.0001$ and $= 0.0047$ for the relative expression levels of *IL1B* and *IL6*, respectively) (Fig. 8k). Additionally, serum lactate levels, assessed upon admission (lactate-1) or within 6 h following antibiotic administration (lactate-2), demonstrated a significant inverse relationship with AAL levels in SPs ($R = -0.23$ and $= -0.2$, $p = 0.035$ and $= 0.073$ for lactate-1 and lactate-2, respectively) (Fig. 8l and Supplementary Fig. 10), suggesting the clinical relevance of AAL levels for sepsis prognosis.

Next, we investigated the role of Fu-Hp in systemic inflammatory responses by injecting it into mice. As shown in Fig. 9a, Fu-Hp significantly elevated the IL-6 and IL-1 β levels in the plasma of mice. Additionally, Fu-Hp considerably increased the mRNA and protein levels of pro-inflammatory cytokines (IL-6, IL-1 β , and TNF- α) in various tissues, including the lung, liver, and spleen, although there was some variation among the cytokines (Fig. 9b). Importantly, Fu-Hp had no effect on the production of the anti-inflammatory cytokine IL-10 (Fig. 9c). These findings indicate that Hp fucosylation has pro-inflammatory effects in vivo and that Fu-Hp-associated gene signatures have potential as prognostic biomarkers for sepsis.

Discussion

Previous studies have demonstrated elevated Hp levels in SPs, with variations depending on clinical severity. Additionally, serum Hp levels have been found to correlate with improved long-term prognosis in patients with septic shock or sepsis^{10,35}. However, the role of Hp glycosylation in complex pathophysiological responses during sepsis remains unclear. In this study, we examined Hp glycosylation profiles in plasma samples from SPs, revealing increased Fu-Hp levels that trigger inflammatory responses. Our investigation in human PBMCs highlighted the critical role of Fu-Hp in inducing a specific subset of macrophages exhibiting robust inflammatory profiles. Fu-Hp increased inflammation, promoted chemokine release, and activated the NLRP3 inflammasome in human primary PBMCs and monocytes. Notably, Fu-Hp-treated PBMCs exhibited upregulated expression of Mincle, a receptor that interacts with Fu-Hp to amplify inflammatory responses. Furthermore, SPs exhibited the presence of a macrophage subpopulation characterized by gene signatures associated with Fu-Hp (including *HP*, *FUT4*, *CLEC4E*, and *IL1B*), while this population was absent in NS-SPs, suggesting its potential utility as a predictive marker for sepsis prognosis.

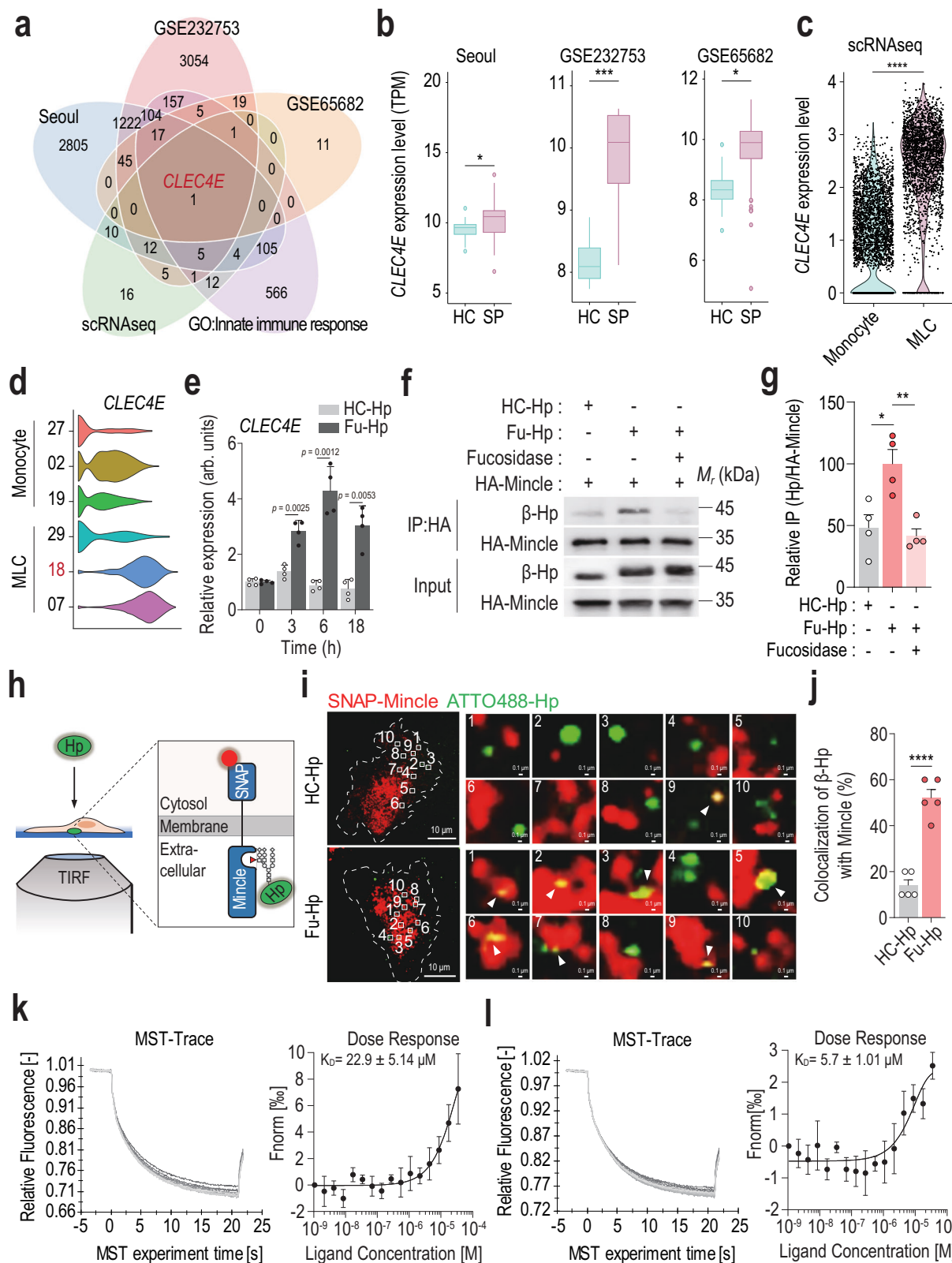
Elevated levels of circulating cell-free Hb in plasma have been associated with inflammation and injury in critically ill patients³⁶. Hp plays a crucial role as a scavenger of cell-free Hb, offering protection in Hb-driven conditions, such as sepsis and hemolysis^{37,38}. Previous research has highlighted Hp's involvement in immune responses triggered by endotoxins, maintaining immune tolerance by suppressing inflammatory mediators³⁹. However, a separate study showed that commercial human Hp therapy did not exhibit clear anti-inflammatory

effects but, instead, showed innate host defense mechanisms in a bacterial pneumonia model⁴⁰. Despite numerous studies suggesting a link between Hp glycosylation and pathological conditions^{2,10,17,41}, the glycosylation profiles in human sepsis remain largely unexplored. Our findings revealed significant increases in specific terminal fucosylation of Hp in plasma from SPs. Moreover, glycoproteomic analysis revealed that fucosylation was specifically increased in tri-/tetra-antennary structures at Asn207 and Asn211 of β -Hp in SP. Given that Hp secreted by hepatocytes exhibited core fucosylation¹⁸, our data suggest that aberrant glycosylation of SP-Hp occurs in different tissues, presumably from distinct monocyte/macrophage subsets (e.g., *FUT4*⁺) during systemic inflammation. Given that the expression levels of *FUT4* and *HP* were specifically increased in a macrophage subset from SPs, β -Hp with sepsis-specific glycosyl-epitopes might be locally secreted by certain immune cells, as is Hp by cancer cells^{18–23}.

CD163, a receptor involved in Hb scavenging, facilitates endocytosis of the Hb-Hp complex, initiating Hb proteolysis and heme catabolism via the heme oxygenase-1 pathway^{42,43}. The interaction between Hb-Hp and CD163-bearing cells stimulates IL-10 secretion, promoting anti-inflammatory and cytoprotective pathways in human monocytes/macrophages⁴⁴. Additionally, a recent study demonstrated that CD163-positive macrophages suppress vascular calcification by enhancing hyaluronan synthase activity⁴⁵. During our search for Fu-Hp binding partners, we discovered an interaction between Fu-Hp and the C-type lectin receptor Mincle/CLEC4E, which was significantly elevated in PBMCs from SPs compared to HCs.

Mincle binds to α -mannose, but not mannan, of *Malassezia* species, and triggers the NFAT-signaling pathways to initiate the production of inflammatory cytokines and chemokines in a manner dependent on Mincle expression³⁴. It binds to ligands such as TDM, β -glucosylceramide, and glucosyl-diacylglycerol, which are found in *Mycobacterium tuberculosis*, *Streptococcus pneumoniae*, and *Candida* species^{46–49}. The binding triggers pro-inflammatory responses via Mincle downstream signaling pathways, including the Fc receptor γ -, NFAT-, and the NF- κ B-signaling pathways, which are crucial for pathogen elimination^{34,50,51}. In the model of sepsis-associated acute kidney injury, the Mincle signaling pathway is closely associated with tubular epithelial cell ferroptosis and contributes to its pathogenesis²⁸. Our data demonstrate that Fu-Hp produced during sepsis can bind to Mincle. This interaction was required for the induction of inflammation and enhanced innate immunity during immunosuppression, implicating Mincle in the maintenance of immune homeostasis. These findings suggest that targeting the Fu-Hp/Mincle interaction could improve the management of sepsis.

Additionally, using shRNA to silence *CLEC4E*, or employing *Clec4e*^{KO} macrophages, significantly inhibited IL-1 β secretion and NLRP3 inflammasome activation. The elevated Mincle levels in SPs, along with its clear association with the inflammatory cytokine IL-1 β ,



suggest that the interaction between Mincle and Fu-Hp contributes to increased inflammation during sepsis. The binding of various receptors to sugars (including C-type lectin receptors, siglecs, and galectins) is important in innate immunity^{52–54}. This study to identifies a ligand, Fu-Hp, that is recognized by a lectin receptor, Mincle, to induce an inflammatory immune response in sepsis. In a recent study, *CLEC5A* was increased in a pro-inflammatory macrophage subset in a sepsis

model⁵⁵, similar to the significant increase in *CLEC5A* in the *CLEC4E*-expressing mlc-18 subset in this study (Supplementary Data 4). Further studies are required to determine whether Fu-Hp is also associated with *CLEC5A*-mediated inflammatory responses during sepsis.

ScRNA-seq data revealed a macrophage population (MLC-18) within Fu-Hp-treated PBMCs from HCs. Previous research has extensively elucidated the heterogeneous composition and disease-specific

Fig. 6 | Mincle receptor is increased and interacts with Fu-Hp. **a** The Venn diagram illustrating the number of genes with significantly increased expression (p value < 0.05) involved in the innate immune response pathway, across three cohorts (Seoul, GSE232753, and GSE65682) and increased genes in the macrophage population of scRNA-seq data. Two-sided p -values were calculated using the likelihood ratio test and adjusted for multiple comparisons using the Benjamini-Hochberg method to control the false discovery rate (FDR). **b**, Box-and-whisker plot showing the expression of the *CLEC4E* gene across three cohorts: Seoul (HCs = 12; SPs = 24), GSE232753 (HCs = 8; SPs = 20), and GSE65682 (HCs = 42; SPs = 479). The lower and upper hinges of the box represent the 25th and 75th percentiles, and the whiskers extend to the minimum and maximum values within 1.5 times the interquartile range. The median value is depicted by the line within the box. Statistical significance was calculated with a two-tailed t -test without adjustment ($*p < 0.05$; $***p < 0.001$). **c** The violin plot depicting expression levels of *CLEC4E* gene in macrophage and monocyte population from PBMCs with or without Fu-Hp treatment. P values were calculated by the FindMarkers function in Seurat 5.0.1 package using the default two-sided Wilcoxon Rank Sum test ($****p < 0.0001$). **d** The violin plot displaying the expression levels of *CLEC4E* gene in subpopulations of monocytes (2, 19, and 27) and macrophages (7, 18, and 29). **e** The relative expression of *CLEC4E* gene in human primary monocytes after treatment with HC-Hp or Fu-Hp for indicated time point using qRT-PCR ($n = 4$ per group). Statistical

significance was calculated with a two-sided unpaired t -test with Sidak-Bonferroni test and presented as means \pm SD. arb. units, arbitrary unit. **f**, Immunoprecipitation assessing the interaction between HA-tagged Mincle and Hp purified from HCs and SPs ($n = 4$ per group). **g** Quantification of β -Hp pulldown by HA-Mincle ($n = 4$ per group). The graph showing the relative intensity of β -Hp bands normalized to HA-Mincle bands. Statistical significance was calculated with an unpaired t -test with Mann-Whitney test and presented as means \pm SEM ($*p < 0.05$; $**p < 0.01$).

h Schematic illustration of examining the interaction using TIRF microscopy. **i**, TIRF microscopy images of SNAP-Mincle and ATTO488-Hp. HeLa cells expressing SNAP-Mincle were labeled with a membrane-impermeable SNAP dye (red) and incubated with ATTO488-labeled HC-Hp or Fu-Hp (green). White arrowheads indicate colocalization of Mincle and Hp. Scale bars, 10 μ m (right) or 0.1 μ m (left). **j**, The bar plot showing the quantitation of colocalization of β -Hp with Mincle ($n = 5$). Statistical significance was calculated with a two-tailed unpaired t -test and presented as means \pm SD ($****p < 0.0001$). **k, l** MST analysis assessing the interaction between HA-tagged Mincle and Hp purified from different cohorts. MST (left) traces and (right) dose response curves were shown. The left panel shows the representative MST trace corresponding to the titration of Hp, and the right panel indicates changes in thermophoresis fitted to yield a KD of $22.9 \pm 5.15 \mu$ M (**k**) and a KD $5.7 \pm 1.01 \mu$ M (**l**). Data are presented as mean \pm standard deviation.

alterations of macrophage subclasses, both in steady-state and various pathological conditions, including sepsis and its complications^{56–58}. Notably, the MLC-18 subset dominated the macrophage landscape, exhibiting the highest upregulation of inflammatory cytokines and chemokines. Furthermore, S-SPs exhibited a distinct macrophage population with Fu-Hp-associated gene signatures (*HP*, *FUT4*, *CLEC4E*, and *IL1B*), whereas this population was absent in NS-SPs.

This study has several limitations that warrant further investigation. First, there is a lack of direct evidence linking specific macrophage subsets, such as FUT4+ macrophages, to the aberrant glycosylation of SP-Hp during systemic inflammation. Further studies are needed to better understand the cellular origins and mechanisms inducing the terminal fucosylation of Hp during sepsis. Second, while the Fu-Hp/Mincle interaction was shown to play a role in Fu-Hp-mediated inflammation, the precise molecular mechanisms underlying this interaction remain unclear. Lastly, the labor-intensive and time-consuming process of isolating Fu-Hp limited the availability of sufficient quantities for extensive in vivo experiments, constraining the ability to thoroughly investigate its systemic effects. Future studies should attempt to generate recombinant Fu-Hp in sufficient amounts to enable in-depth investigation of its functions in vivo at clinically relevant levels. In summary, our study revealed that the Fu-Hp level is elevated during sepsis, exhibits correlations with inflammatory markers including IL-1 β and IL-6, and interacts with and signals through Mincle. These findings suggest the feasibility of targeted interventions for sepsis based on the modulation of terminal Hp fucosylation.

Methods

Study design

All patients with sepsis and septic shock enrolled between May 2018 and March 2024 provided written informed consent before enrollment, and the trial was registered at ClinicalTrials.gov (NCT05911711). Patients admitted to the medical ICUs of the following hospitals were screened daily for inclusion and exclusion criteria: Kangdong Sacred Heart Hospital, Chungnam National University Hospital, and Ewha Womans University Seoul Hospital. At Chungnam National University Hospital, 18 participants were recruited from May 25, 2018, to January 2, 2019, and an additional 6 participants were recruited from March 24, 2023, to June 23, 2023. At Ewha Womans University Seoul Hospital, 42 participants were recruited from May 8, 2019, to January 8, 2022.

At Kangdong Sacred Heart Hospital, 86 participants were recruited from May 30, 2022, to March 6, 2024. A normal control group was

enrolled between May 2018 and March 2024 from Chungnam National University Hospital. This research adhered to the principles outlined in the Helsinki Declaration and the protocol was approved by the institutional review board (IRB) of each participating center (IRB no. 2018-03-058 from Chungnam National University Hospital; no. 2019-10-011-017 from Ewha Womans University Medical Center; and no. 2022-03-015-006 from Kangdong Sacred Heart Hospital). All other data are available in the main text, supplementary information (Supplementary Data 1).

Enrollment criteria included the following: age > 18 years of age with admission to ICU, with sepsis or septic shock who was expected to required close monitoring or invasive treatment (mechanical ventilation, continuous renal replacement therapy, extracorporeal membranous oxygenation, polymyxin hemoperfusion B, inotropics or vasopressor use) as judged by the treating ICU specialist. Sex or gender was not considered in the study design.

The exclusion criteria were as follows: the patient or caregiver does not agree to participate in the study, the patient has undergone a bone marrow or organ transplant, the patient has a Do Not Resuscitate (DNR) order, the patient is under the age of 18.

Blood collection

We collected 6–9 mL blood samples from healthy donor or sepsis patients using Vacutainer Sodium Heparin (BD, 367955). The blood samples were centrifuged 10 mL of blood at $1000 \times g$ for 3 min to separate and store 1 mL plasma at -80°C until analysis.

Cell preparation

Human PBMCs were isolated using LymphoprepTM (STEMCELL, 07851). The isolated human PBMCs were stored via Cell banker 1 (Zenoaq, BLC-1) at 3×10^6 cells per mL for bulk RNA and scRNA sequencing. Human monocytes/macrophages were prepared using CD14 MicroBeads (Miltenyi Biotech, 130-050-201). These cells were cultured in RPMI 1640 (Sigma-Aldrich) with 10 % heat-inactivated fetal bovine serum (Gibco). HeLa cells were from ATCC and cultured in complete DMEM containing 10 % FBS. THP-1 cells were cultured in RPMI 1640 and treated with 500 nM phorbol myristol acetate for 24 h to differentiated to macrophages, then rested for 24 h before assay. Mouse bone marrow-derived macrophages were obtained from the 8-week-old C57BL/6 wild-type (Samtako Bio) or *Clec4e*^{-/-} from female mice and cultured in DMEM with 10 % heat-inactivated fetal bovine serum (Gibco).

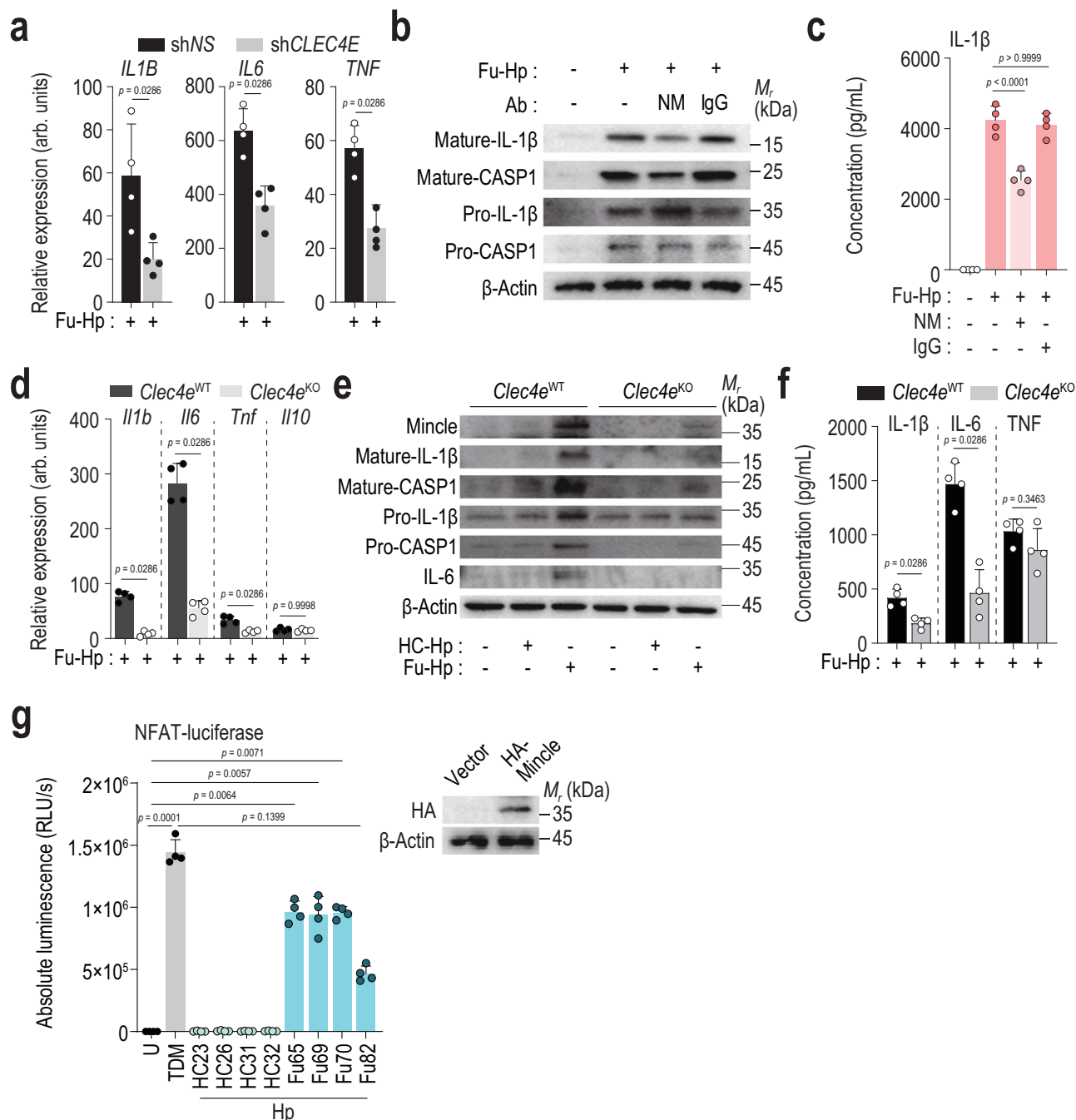


Fig. 7 | Mincle is required for Fu-Hp-induced proinflammatory cytokine expression and NLRP3 inflammasome activation. **a** The relative expression of indicated genes after Fu-Hp treatment in nonspecific (shNS) or *CLEC4E* knockdown (sh*CLEC4E*) monocytes using qRT-PCR ($n = 4$ per group). Statistical significance was calculated with a one-way ANOVA with Bonferroni test and presented as means \pm SD. arb. units, arbitrary unit. **b** Western blotting for mature IL-1 β , mature caspase1, pro-IL-1 β , IL-6, and pro-caspase1 in human primary monocytes treated for 18 h with Fu-Hp. NM, Human Mincle neutralizing antibody; IgG, Mouse Control IgG2b. **c**, The concentrations of IL-1 β in the supernatants of human primary monocytes with Fu-Hp treatment after indicated antibodies (NM or IgG) pretreatment measured by ELISA ($n = 4$ per group). Statistical significance was calculated with a two-sided unpaired *t*-test with Mann-Whitney test and presented as means \pm SD. **d**, The relative expression of indicated genes after Fu-Hp treatment in mouse BMDM from *Clec4e*^{WT} or *Clec4e*^{KO} using qRT-PCR ($n = 4$ per group). Statistical significance was

calculated with a two-sided unpaired *t*-test with Mann-Whitney test and presented as means \pm SD. arb. units, arbitrary unit. ns, not significant. **e** Western blotting for mature IL-1 β , mature caspase1, pro-IL-1 β , IL-6, and pro-caspase1 in mouse BMDM from *Clec4e*^{WT} or *Clec4e*^{KO} treated for 18 h with Fu-Hp. **f** The concentrations of IL-1 β , IL-6, and TNF in the supernatants of Fu-Hp-treated *Clec4e*^{WT} or *Clec4e*^{KO} BMDM (100 μ g/mL for 18 h) measured by ELISA ($n = 4$ per group). ns, not significant. Statistical significance was calculated with a two-sided unpaired *t*-test with Mann-Whitney test and presented as means \pm SEM. **g** Firefly luciferase reporter vector (NFAT-RE) were stimulated with HC-Hp or Fu-Hp, and reporter assay was performed in HeLa cells transfected with a HA-Mincle expression vector (left; $n = 4$ per group). HA-Mincle transfection was confirmed by WB using an HA antibody (right). Statistical significance was calculated with a two-sided Kruskal-Wallis test and presented as means \pm SD. RLU/s, Relative Light Units per second.

Fig. 8 | Fu-Hp-associated of gene signatures are associated with prognosis of SP. **a** Bar plot of the proportion of cell types in scRNA-seq data of HCs and SPs, separated by two HC samples and two SP samples. HC, Healthy control; S-SP, Surviving patients; NS-SP, Non-surviving patients. **b** The UMAP plot illustrating the alterations in cell proportions between SP and HC. **c**, Bar plot of the proportion of indicated cell types shown in **a** and **b**, separated by groups. HC, Healthy control; SP, Sepsis patients; MLC-NS, Macrophage-like cell population from non-surviving patient; MLC-S, Macrophage-like cell population from surviving patient. **d** The violin plot depicting expression levels of indicated genes in MLC-S and MLC-NS ($\log_2(\text{fold change}) > 0.5$). *P* values were calculated by the FindMarkers function in Seurat 5.0.1 package using the default two-sided Wilcoxon Rank Sum test (*****p* < 0.0001). ns, not significant; MLC-NS, Macrophage-like cell population from non-surviving patient; MLC-S, Macrophage-like cell population from surviving patient. **e** Unsupervised UMAP analysis on PBMCs pooled from 2 HC and 10 SP (6 surviving patients and 4 deceased patients) in public sepsis cohort (GSE167363). Cell populations were mapped onto the UMAP landscape to visualize the distribution of cells across clusters. **f** Bar plot of the proportion of indicated cell types shown in **e**, separated by samples. HC, Healthy control; S, Surviving patients; NS, Non-surviving patients. **g** Bar plot depicting of the cell count of cluster 3 shown in **f**, separated by patient groups. S-SP, Surviving sepsis patients; NS-SP, Non-surviving sepsis patients (*n* = 6 for S; *n* = 4 for NS). Statistical significance was calculated with a two-tailed unpaired *t*-test with Mann-Whitney test and presented as means \pm SD (**p* < 0.05). **h** Volcano plot depicting DEGs between cluster 3 and other clusters in

GSE167363. Gene signatures were labeled (adjusted *p* values < 0.04³⁰¹). *P* values were calculated by the FindMarkers function in Seurat 5.0.1 package using the default two-tailed Wilcoxon Rank Sum test. **i, j** Box-and-whisker plot illustrating the expression of the indicated genes in Seoul cohort (*n* = 12 for HC; *n* = 19 for S; *n* = 5 for NS). The lower and upper hinges of the box represent the 25th and 75th percentiles, and the whiskers extend to the minimum and maximum values within 1.5 times the interquartile range. The median value is depicted by the line within the box. Statistical significance was calculated with a two-tailed *t*-test without adjustment (***p* < 0.01; ****p* < 0.001; *****p* < 0.0001). ns, not significant; HC, Healthy control; S, Surviving patients; NS, Non-surviving patients. **k** Correlation between the expression of the AAL level (x-axis) and the expression of either the relative expression of indicated genes (*IL1B* and *IL6*) (y-axis) with the best linear fit plotted in our cohort (*n* = 23 for HC; *n* = 24 for S; *n* = 12 for NS). Pearson's correlation coefficient and the *p* value are displayed in the bottom-right corner. The shaded area represents the 95 % confidence interval. *P* values were calculated using a *t*-distribution with [*n*-2] degrees of freedom. HC, Healthy control; S, Surviving patients; NS, Non-surviving patients. **l** Correlation between the expression of the AAL level (x-axis) and the level of lactate-1 (y-axis) with the best linear fit plotted in our cohort (*n* = 84 for S; *n* = 33 for NS). Pearson's correlation coefficient and the *p* value are displayed in the top-right corner. The shaded area represents the 95 % confidence interval. *P* values were calculated using a *t*-distribution with [*n*-2] degrees of freedom. S, Surviving patients; NS, Non-surviving patients.

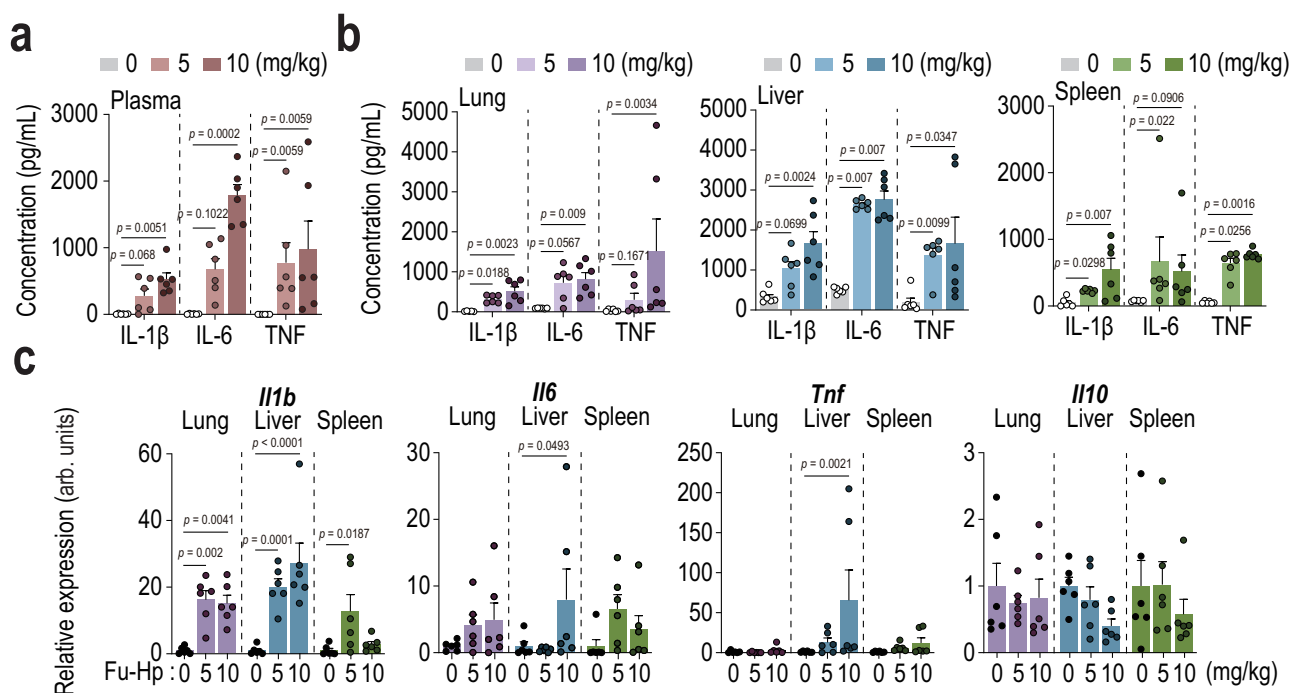


Fig. 9 | Administration of Fu-Hp in mice leads to the upregulation of pro-inflammatory cytokine expression in vivo. **a** The concentrations of IL-1 β , IL-6, and TNF were measured by ELISA in plasma of female 8-week-old C57BL/6 mice following Fu-Hp administration (*n* = 6 per group). Statistical significance was calculated with a Kruskal-Wallis test with Dunn's test and presented as means \pm SEM. ns, not significant. **b** The concentrations of IL-1 β , IL-6, and TNF were measured by ELISA in indicated organ of female 8-week-old C57BL/6 mice following Fu-Hp

administration (*n* = 6 per group). Statistical significance was calculated with a two-sided unpaired *t*-test with Mann-Whitney test and presented as means \pm SEM. ns, not significant. **c** The relative expression of indicated genes in indicated organ of female 8-week-old C57BL/6 mice following Fu-Hp administration (*n* = 6 per group). Statistical significance was calculated with a two-way ANOVA with Bonferroni's test and presented as means \pm SEM.

and 5 % glycerol) containing a protease inhibitor cocktail (Sigma-Aldrich). After centrifugation at 2,000 \times g for 30 min, the supernatant was subjected to Ni-NTA column (Qiagen). 6x his-tagged β -Hp was eluted with elution buffer (20 mM Tris-HCl at pH 8.0, 150 mM NaCl, 300 mM imidazole, 1 mM DTT, and 5 % glycerol). The purified β -Hp was dialyzed with PBS buffer, quantified using Bradford assay (Thermo Fischer Scientific), and stored at -80°C until use.

Lectin blotting analysis

We used lectin blotting to evaluate Hp glycosylation²⁴. 2 μ g of Hp was subjected to SDS-PAGE and transferred into polyvinylidene difluoride (PVDF) membrane (Millipore). After blocking with 3 % BSA in TBS-T (20 mM Tris-HCl pH7.4, 150 mM NaCl, 0.9 mM CaCl₂, 0.5 mM MgSO₄, 0.1 mM MnCl₂ and 0.5 % Tween-20), the membranes were incubated with biotinylated lectins (AAL, 1:1000; SNA, 1:1000; PHAL, 1:500;

VectorLabs) at 4 °C, overnight. After 3x washing with TBS-T, the membrane was incubated with streptavidin-HRP (1:10,000, Sigma Aldrich) at RT for 30 min. After 3x washing with TBS-T, the membrane was developed with ECL solution (Enzymomics) and visualized using the Fusion Solo S (Vilber). For reblotting to detect Hp signals, the membrane was incubated with stripping buffer (LPS solution) for 1 h at RT. After blocking with 5 % skim milk in TBS-T (20 mM Tris-HCl pH7.4, 150 mM NaCl, and 0.5 % Tween-20), the membrane was incubated with rabbit anti-Hp antibody (1:2,000, Sigma-Aldrich) at 4 °C overnight. Following washing with TBS-T, the membranes were incubated with HRP conjugated goat anti-rabbit IgG for 1 h at RT. The membrane was developed using ECL solution.

LC (GC)-ESI MS analysis for desialo-glycans of Hp

10 µg of Hp purified from human sera was dotted on PVDF membrane. N-glycans were released with PNGaseF from dotted Hp⁵⁹. The released N-glycans were desialylated with acetic acid before labelling with aminoxymethylamine reagent (aTMT, Thermo Fisher Scientific)⁶⁰. Finally, the samples were analyzed by LC (GC)-ESI MS⁶⁰. The procedure for sample preparation of desialo-glycan of Hp, analytical conditions of LC-ESI MS and data analysis were performed according to previous report^{59,60}. The peak intensities of each N-glycan labeled with aTMT6 were calculated on the extracted-ion chromatogram (± 6 ppm of theoretical mass) using Xcalibur software version 2.2 (Thermo Fisher Scientific). The relative abundances (%) of each glycan structure were calculated by setting the total peak intensities of all detected aTMT6-labeling N-glycans in each extracted ion chromatogram (EIC) to 100 %.

LC (ODS)-ESI MS analysis for desialo-glycopeptides of Hp

90 µg of Hp purified from human sera was digested with trypsin and endoprotease Glu-C after reduction with DTT and alkylation with IAA²⁰. The glycopeptides were desialylated with acetic acid after enrichment with Sepharose²⁰. Finally, the samples were analyzed by LC (ODS)-ESI MS²⁵. The procedure for sample preparation of desialo-glycopeptide of Hp, analytical conditions of LC-ESI MS and data analysis were performed according to previous report^{20,25}. The peak intensities of each glycopeptide were calculated on the extracted-ion chromatogram (± 6 ppm of theoretical mass) using Xcalibur software version 2.2 (Thermo Fisher Scientific). The relative abundances (%) of each glycan structure on glycopeptide were calculated by setting the total peak intensities of all detected glycopeptides in each extracted ion chromatogram (EIC) to 100 %.

Bulk RNA-sequencing Analysis

RNA sequencing was performed on PBMCs from HC and SP to examine the different gene expression and ontology pathway analysis. Briefly, RNA-seq libraries were prepared using a SureSelect^{XT} RNA Direct Reagent Kit (Agilent Technologies, G7564B). Total RNA was extracted from PBMCs using TRIzol[®] Reagent (Thermo Fisher, 15596026) according to the manufacturer's instructions. Transcriptome library sequencing was carried out using the 101-bp paired-end mode with Illumina NovaSeq 6000. The data integrity of the raw sequences was evaluated with FastQC v0.11.7 (<http://www.bioinformatics.babraham.ac.uk/projects/fastqc/>). The raw read data were trimmed using Trimmomatic (version 0.38) and the following criteria: first trimming: base quality < 3, window size = 4, and mean quality = 15; second trimming: min length = 36 bp. The trimmed reads were mapped against the reference genome GRCh38 using HISAT2 version 2.1.0 (<https://ccb.jhu.edu/software/hisat2/index.shtml>) and Bowtie2 aligner. After the read mapping, StringTie (version 2.1.3b) was used for transcript assembly. The expression profile was calculated for each sample and transcript/gene as read count, FPKM (Fragment per Kilobase of transcript per Million mapped reads) and TPM (Transcripts Per Kilobase Million). DEG (Differentially Expressed Genes) analysis was performed on a

comparison pair (Sepsis patients vs Healthy control) using DESeq2. The statistical method used was calculated based on fold change, `nbinomWaldTest` using DESeq2, and Hierarchical Clustering. Using each sample's normalized value, the high expression similarities were grouped together. The significant results are selected on conditions of the absolute value of $|\log_2(\text{fold change})| \geq 2$ & `nbinomWaldTest` raw p value < 0.05. Normalized gene expression values were utilized to generate a heatmap using the `pheatmap` package (version 1.0.12) and a volcano plot employing the `ggplot2` package (version 3.4.4) within the R programming environment (version 4.1.3). Pathway enrichment analysis was conducted using the `clusterProfiler` package (version 4.10.0) in R and the Gene Set Enrichment Analysis (GSEA) software (version 4.3.2).

RNA extraction and qRT-PCR

Total RNA was extracted using TRIzol[®] Reagent (Thermo Fisher, 15596026) according to the protocol provided by the manufacturer. Subsequent to RNA extraction, first-strand cDNA synthesis was carried out using Reverse Transcriptase Premix (ELPIS Biotech, EBT-1515) following the manufacturer's guidelines. For quantitative real-time PCR (qRT-PCR), SYBR[®] Green PCR Master Mix (Qiagen, 204074) was utilized in a Rotor-Gene Q 2plex system (Qiagen). Gene expression analysis was performed using the $2^{-\Delta\Delta C_t}$ method, with GAPDH serving as the normalization control. Primer sequences for qRT-PCR were listed in Supplementary Table 2.

Enzyme-Linked Immunosorbent Assays (ELISA)

The concentration of human IL-1 β , human IL-6, human TNF, mouse IL-6, and mouse TNF were assayed with BD OptEIA Set ELISA Kits (BD, 557953; 555220; 555212; 555240; 560478). The concentration of mouse IL-1 β was assessed with IL-1 beta mouse ELISA Kit (Thermo Fisher Scientific, BMS6002), following the manufacturer's protocol. Samples were assayed with up to 50-fold dilution and incubated overnight at 4 °C. Samples were assayed in triplicates, and the mean of the triplicate values was used in statistical analysis.

Immunoblotting

Immunoblotting was performed using NuPAGE 8 - 15 % Bis-Tris polyacrylamide gels for the electrophoretic separation of proteins. After electrophoresis, proteins were transferred onto PVDF membranes via a semi-dry transfer method (Bio-Rad). Membranes were then blocked in a solution of 5 % skim milk in Tris-buffered saline containing 0.1 % Tween 20. Primary antibodies were incubated under gentle agitation overnight at 4 °C. The antibodies varied in the concentration and were specific to antigens (Supplementary Table 3). HRP-conjugated secondary antibodies were used at dilutions of either 1:2,000 or 1:5,000 depending on the primary antibody (Supplementary Table 3). For detecting the mature IL-1 β and mature Caspase-1, cell culture supernatants were precipitated using StrataClean Resin (Agilent Technologies, 400714). StrataClean Resin was added, mixed well by vortexing for 1 min, and centrifuged at 210 \times g for 2 min at 4 °C. After discarding the supernatant, resin-binding proteins were harvested by boiling for 7 min in 1 \times SDS loading buffer⁶¹. All original immunoblotting membrane data can be found in the Source Data file.

Single-cell RNA-sequencing analysis

Each cell was tagged with antibody-polyadenylated DNA barcode for human cells (BD Biosciences, 633781). Concisely, we bound the cells with multiplexing antibody for 30 min at room temperature (RT), and then washed the cells using stain buffer 3 times (BD Biosciences, 554656). After washing, cells were gently resuspended in cold sample buffer (BD Biosciences, 664887), counted with a LUNA-FX7[™] Automated Fluorescence Cell Counter (logos biosystems), and then pooled. We performed the single cell capture using BD Rhapsody Express

instrument according to the manufacturer's protocol (BD Bioscience). ScRNA-seq libraries were constructed using BD Rhapsody WTA amplification kit (BD Biosciences, 633801). The purified WTA and Sample tag libraries were quantified using qPCR according to the qPCR Quantification Protocol Guide (KAPA), and qualified using the Agilent Technologies 4200 TapeStation (Agilent technologies). The libraries were sequenced using NovaSeq platform (Illumina). The raw sequencing data (FASTQ) was processed using the BD Rhapsody WTA Analysis Pipeline v2.0 (BD Biosciences) and aligned against the human reference data (GRCh38). Seurat (version 5.0.1) was used for Dimensionality reduction, cell clustering, calculating module score, and differential gene expression analysis.

CLEC4E knockdown

Short hairpin RNA (shRNA) targeting *CLEC4E* (sc-95678-SH) was purchased from Santa Cruz Biotechnology. Non-silencing lentivirus shRNA (scrambled control; sc-108060) was used as control. For the study, THP-1 cells and human primary monocytes were cultured in 24 or 48-well plates and transduced with the lentiviral shRNA vectors for a period of 36 h prior to Hp treatment. qPCR was used to determine the knockdown efficiency.

Clec4e knockout mice

Clec4e^{-/-} mice were backcrossed for at least 23 generations with C57BL/6 mice. All mice were maintained in a filtered-air laminar-flow enclosure and given standard laboratory food and water ad libitum as previously described³⁴. All animal procedures were approved by the Committee of Ethics on Animal Experiments at the Research Institute for Microbial Diseases, Osaka University, Japan (Biken-AP-R03-17-0).

Mouse models

The treatment of mice was conducted in compliance with the guidelines set by the Institutional Animal Care and Use Committee of Chungnam National University School of Medicine (202109A-CNU-180), as well as the regulations established by the Korean Food and Drug Administration. All experiments were performed using 6–8 week old male or female C57BL/6 mice obtained from Samtako Bio. Mice were housed in a specific pathogen-free facility with a 12-hour light/dark cycle. Mice were euthanized by carbon dioxide inhalation followed by cervical dislocation.

To investigate the effects of Fu-Hp in mice, we conducted an experiment using 8-week-old female C57/BL6 mice. The mice were divided into three groups ($n = 6$ per group) and given either a control injection of PBS, or Fu-Hp (5 mg/kg or 10 mg/kg) intraperitoneally. 2 h after the injections, blood samples were collected from all mice. Following this, liver, lung, and spleen tissues were harvested for analysis. Mouse blood was collected into BD Vacutainer® SST™ II Advance tubes (BD Bioscience, 367955). After collection, tubes were gently inverted 4–6 times and allowed to clot for 30 min at RT. Serum was separated by centrifugation at $1000 \times g$ for 10 min at RT. Separated serum was then used for ELISA. Lung, liver, and spleen tissues were homogenized and then used for RNA preparation and ELISA.

Immunoprecipitation

Hela cells were transfected with HA-Mincle using GenJet™ (SignaGen Lab, SL100489) for 2 days. After lysing the cells with lysis buffer (20 mM Tris-HCl at pH 8.0, 150 mM NaCl, 1 % Triton X-100, and protease inhibitor), Mincle was purified by incubating with anti-HA antibody on protein G PLUS-agarose beads (Santa Cruz Biotechnology, sc-2002) at 4 °C, overnight. The beads were washed twice using lysis buffer and then incubated with 1.5 µg of β-Hp, purified from human sera in 500 µL of reaction buffer (10 mM HEPES, 140 mM NaCl, 2 mM CaCl₂, 1 mM MgCl₂, 0.1 % Triton X-100 and protease inhibitor) for 3 h at RT. The beads were rinsed three times using reaction buffer, and then subjected to Western blotting using rabbit anti-Hp antibody (1:2000,

Sigma-Aldrich) and rabbit anti-HA antibody (1:1,000, Sigma-Aldrich). The PVDF membrane was developed using ECL solution (Enzygnomics) and visualized using the Fusion Solo S (Vilber).

Luciferase assay

To investigate the binding of Fu-Hp to Mincle receptors, we obtained the pGL4.32[luc2P/NFAT-RE/Hygro] vector (Promega, E8481) from the Prof. Hong Sung-Tae's laboratory. Transfection of HeLa cells was performed in four replicates in 96-well plates using Lipofectamine 3000 transfection reagent (Thermo-Fisher, L3000150). The reaction mixture consisted of Lipofectamine 3000 with 0.4 µL of P3000™ Reagent, 0.3 µL of Lipofectamine™ 3000 Reagent, 100 ng HA-Mincle overexpression vector and 100 ng of NFAT reporter vector per well. Luciferase assays were performed with a Bright-Glo™ Luciferase Assay System (Promega, E2610) using a LUMIstar OMEGA Microplate reader (BMG Labtech).

TIRF microscopy

Hela cells on glass coverslips were transfected with SNAP-Mincle using GenJet™ (SignaGen Lab, SL100489) for 2 days. Cells expressing SNAP-Mincle were incubated with 2.5 µg of Hp pre-labeled with ATTO 488 (ATTO-TEC) for 2 h at 37 °C. Cells were rinsed twice with PBS and fixed with 4 % PFA for 15 min at RT. SNAP-Mincle was stained using SNAP-Cell 647-SIR (NEB) for 15 min at RT. Cells were imaged with TIRF microscopy, where 488 nm laser was used to detect Hp and 647 nm laser was used to detect SNAP-Mincle⁶². The colocalization between Mincle and Hp was quantified using image J.

MicroScale Thermophoresis

Hela cells were transfected with HA-Mincle using GenJet™ (SignaGen Lab, SL100489) for 2 days. After lysing the cells with lysis buffer (20 mM Tris-HCl at pH 8.0, 150 mM NaCl, 1 % Triton X-100, and protease inhibitor), Mincle was purified by incubation with anti-HA antibody on protein G PLUS-agarose beads (Santa Cruz Biotechnology, sc-2002) at 4 °C overnight. The beads were washed once with PBS and then labeled with Alexa Fluor™ 647 NHS Ester (Thermo Fisher Scientific) for 1 h at RT. After washing the beads with PBS, the labeled Mincle was eluted using elution buffer (0.1 M glycine, 0.5 M NaCl, pH 2.8). The eluent was then dialyzed with reaction buffer (50 mM HEPES at pH 7.5, 200 mM NaCl, 1 mM MgSO₄, 2 mM CaCl₂). To monitor the interaction of Hp with Mincle by microscale thermophoresis, a series of 16 sequential 1:1 dilutions of Hp were prepared in reaction buffer, producing concentrations ranging from 70 µM to 0.5 nM. For the binding assay, 10 nM of labelled Mincle was mixed with each Hp dilutions at a 1:1 volume ratio, resulting in final concentrations of 5 nM labelled Mincle and 35 µM to 0.25 nM Hp. After incubating for 30 min at RT, the mixtures were loaded into Monolith NT.115 capillaries (NanoTemper), and thermophoresis was measured using a Monolith NT.115 instrument (NanoTemper).

Confocal microscopy

The coverslips were incubated with Poly-L-lysine solution (PLL) (Sigma Aldrich; P4832) for 2 h at RT. The coverslips were washed by PBS and culture media 2 times and dried for 1 h. The 24-well culture plate was seeded the 1×10^5 monocytes on a PLL-coated coverslip. Cells were stained with DAPI and MitoSOX for detecting the mitochondria ROS. Cells were incubated with p65 antibody (1:500; Santa Cruz Biotechnology; sc-8008) for 18 h at 4 °C. Following three washes in the TBS-T, the primary antibody binding was visualized by incubation with Alexa Fluor® 488 conjugate- secondary antibody (1:500; Thermo Fischer Scientific; A-11029) diluted in the washing solution for 2 h at RT.

Statistical Analysis

Statistical analyses were performed using GraphPad Prism 10 (Graphpad Software, version 10.2.0). *P* values were calculated by one-way

analysis of variance (ANOVA) with Tukey or Bonferroni's multiple comparison test or unpaired t-test with the Mann-Whitney test. All statistical tests are indicated in the figure legends. The n values represent the number of independent biological replicates.

Reporting summary

Further information on research design is available in the Nature Portfolio Reporting Summary linked to this article.

Data availability

The transcriptomic sequencing data (Seoul cohort and Hp-treated PBMCs) used in this study have been deposited in NCBI Gene Expression Omnibus (GEO; [GSE270838](https://www.ncbi.nlm.nih.gov/geo/query/acc.cgi?acc=GSE270838); [GSE286141](https://www.ncbi.nlm.nih.gov/geo/query/acc.cgi?acc=GSE286141)). The scRNA-seq data (Fu-Hp-treated PBMCs and sepsis patients) have been deposited in NCBI GEO [GSE286921](https://www.ncbi.nlm.nih.gov/geo/query/acc.cgi?acc=GSE286921) and [GSE286922](https://www.ncbi.nlm.nih.gov/geo/query/acc.cgi?acc=GSE286922). In addition, the publicly available bulk RNA-seq and microarray data used in this study are accessible at NCBI GEO ([GSE232753](https://www.ncbi.nlm.nih.gov/geo/query/acc.cgi?acc=GSE232753) [<https://www.ncbi.nlm.nih.gov/geo/query/acc.cgi?acc=GSE232753>] and [GSE154918](https://www.ncbi.nlm.nih.gov/geo/query/acc.cgi?acc=GSE154918) for bulk RNA-seq; [GSE65682](https://www.ncbi.nlm.nih.gov/geo/query/acc.cgi?acc=GSE65682) for microarray). Also, publicly available scRNA-seq data of sepsis patients are accessible at NCBI GEO ([GSE167363](https://www.ncbi.nlm.nih.gov/geo/query/acc.cgi?acc=GSE167363) [<https://www.ncbi.nlm.nih.gov/geo/query/acc.cgi?acc=GSE167363>]). Glycomic and glycoproteomic raw data and result files by LC-ESI MS have been deposited to the GlycoPOST (GPST000533 [<https://glycopost.glycosmos.org/entry/GPST000533>]). All other data are available in the article and its Supplementary files or from the corresponding author upon request. Source data are provided with this paper.

Code availability

All R code used in this study for analysis is available at the following address: https://github.com/rtaylor0545/JEK232-Lab/tree/7c41b91f4205a2f4988782bac4e34de9cbb0fa21/Rcode_for_Fu-Hp.

References

- Kristiansen, M. et al. Identification of the haemoglobin scavenger receptor. *Nature* **409**, 198–201 (2001).
- Tamara, S., Franc, V. & Heck, A. J. R. A wealth of genotype-specific proteoforms fine-tunes hemoglobin scavenging by haptoglobin. *Proc. Natl Acad. Sci. USA* **117**, 15554–15564 (2020).
- Van Vlierberghe, H., Langlois, M. & Delanghe, J. Haptoglobin polymorphisms and iron homeostasis in health and in disease. *Clin. Chim. Acta* **345**, 35–42 (2004).
- Reinhart, K. et al. Recognizing Sepsis as a Global Health Priority - A WHO Resolution. *N. Engl. J. Med* **377**, 414–417 (2017).
- Harris, E. CDC Introduces Hospital Sepsis Program Guidelines. *JAMA* **330**, 1128 (2023).
- Rudd, K. E. et al. Global, regional, and national sepsis incidence and mortality, 1990–2017: analysis for the Global Burden of Disease Study. *Lancet* **395**, 200–211 (2020).
- Giamarellos-Bourboulis, E. J. et al. The pathophysiology of sepsis and precision-medicine-based immunotherapy. *Nat. Immunol.* **25**, 19–28 (2024).
- Guo, P., Wang, R., Shen, J., Zhang, L. & Mo, W. Identification of Key Inflammation-related Genes as Potential Diagnostic Biomarkers of Sepsis. *Alter. Ther. Health Med* **29**, 24–31 (2023).
- Janz, D. R. et al. Association between haptoglobin, hemopexin and mortality in adults with sepsis. *Crit. Care* **17**, R272 (2013).
- Lan, P., Yu, P., Ni, J. & Zhou, J. Higher serum haptoglobin levels were associated with improved outcomes of patients with septic shock. *Crit. Care* **26**, 131 (2022).
- Opdenakker, G., Rudd, P. M., Ponting, C. P. & Dwek, R. A. Concepts and principles of glycobiology. *FASEB J.* **7**, 1330–1337 (1993).
- Rudd, P. M., Elliott, T., Cresswell, P., Wilson, I. A. & Dwek, R. A. Glycosylation and the immune system. *Science* **291**, 2370–2376 (2001).
- Chen, Y., Hojo, S., Matsumoto, N. & Yamamoto, K. Regulation of Mac-2BP secretion is mediated by its N-glycan binding to ERGIC-53. *Glycobiology* **23**, 904–916 (2013).
- Boscher, C., Dennis, J. W. & Nabi, I. R. Glycosylation, galectins and cellular signaling. *Curr. Opin. Cell Biol.* **23**, 383–392 (2011).
- Ackerman, M. E. et al. Natural variation in Fc glycosylation of HIV-specific antibodies impacts antiviral activity. *J. Clin. Invest* **123**, 2183–2192 (2013).
- Taniguchi, N. & Kizuka, Y. Glycans and cancer: role of N-glycans in cancer biomarker, progression and metastasis, and therapeutics. *Adv. Cancer Res* **126**, 11–51 (2015).
- Oh, M. J., Lee, S. H., Kim, U. & An, H. J. In-depth investigation of altered glycosylation in human haptoglobin associated cancer by mass spectrometry. *Mass Spectrom. Rev.* **42**, 496–518 (2023).
- Ang, I. L. et al. Study of serum haptoglobin and its glycoforms in the diagnosis of hepatocellular carcinoma: a glycoproteomic approach. *J. Proteome Res* **5**, 2691–2700 (2006).
- Miyoshi, E. & Nakano, M. Fucosylated haptoglobin is a novel marker for pancreatic cancer: detailed analyses of oligosaccharide structures. *Proteomics* **8**, 3257–3262 (2008).
- Nakano, M. et al. Site-specific analysis of N-glycans on haptoglobin in sera of patients with pancreatic cancer: a novel approach for the development of tumor markers. *Int. J. Cancer* **122**, 2301–2309 (2008).
- Park, S. Y. et al. alpha1-3/4 fucosylation at Asn 241 of beta-haptoglobin is a novel marker for colon cancer: a combinatorial approach for development of glycan biomarkers. *Int. J. Cancer* **130**, 2366–2376 (2012).
- Park, S. Y. et al. N-glycosylation status of beta-haptoglobin in sera of patients with colon cancer, chronic inflammatory diseases and normal subjects. *Int. J. Cancer* **126**, 142–155 (2010).
- Ferens-Sieczkowska, M., Kratz, E. M., Kossowska, B., Passowicz-Muszynska, E. & Jankowska, R. Comparison of haptoglobin and alpha(1)-acid glycoprotein glycosylation in the sera of small cell and non-small cell lung cancer patients. *Postepy Hig. Med Dosw (Online)* **67**, 828–836 (2013).
- Choi, H. et al. Terminal fucosylation of haptoglobin in cancer-derived exosomes during cholangiocarcinoma progression. *Front Oncol.* **13**, 1183442 (2023).
- Takahashi, S. et al. Site-specific and linkage analyses of fucosylated N-glycans on haptoglobin in sera of patients with various types of cancer: possible implication for the differential diagnosis of cancer. *Glycoconj. J.* **33**, 471–482 (2016).
- Lu, X., Nagata, M. & Yamasaki, S. Mincle: 20 years of a versatile sensor of insults. *Int. Immunol.* **30**, 233–239 (2018).
- Richardson, M. B. & Williams, S. J. MCL and Mincle: C-Type Lectin Receptors That Sense Damaged Self and Pathogen-Associated Molecular Patterns. *Front Immunol.* **5**, 288 (2014).
- Zhang, J. et al. SAP130 released by ferroptosis tubular epithelial cells promotes macrophage polarization via Mincle signaling in sepsis acute kidney injury. *Int. Immunopharmacol.* **129**, 111564 (2024).
- Lee, W. B. et al. Mincle activation enhances neutrophil migration and resistance to polymicrobial septic peritonitis. *Sci. Rep.* **7**, 41106 (2017).
- Sharma, A., Steichen, A. L., Jondle, C. N., Mishra, B. B. & Sharma, J. Protective role of Mincle in bacterial pneumonia by regulation of neutrophil mediated phagocytosis and extracellular trap formation. *J. Infect. Dis.* **209**, 1837–1846 (2014).
- Singer, M. et al. The Third International Consensus Definitions for Sepsis and Septic Shock (Sepsis-3). *JAMA* **315**, 801–810 (2016).
- Hu, Z. et al. Dissecting the single-cell transcriptome network of macrophage and identifies a signature to predict prognosis in lung adenocarcinoma. *Cell Oncol. (Dordr.)* **46**, 1351–1368 (2023).

33. Bird, J. H. et al. Synthesis of Branched Trehalose Glycolipids and Their Mincle Agonist Activity. *J. Org. Chem.* **83**, 7593–7605 (2018).
34. Yamasaki, S. et al. C-type lectin Mincle is an activating receptor for pathogenic fungus, *Malassezia*. *Proc. Natl Acad. Sci. USA* **106**, 1897–1902 (2009).
35. Mizuno, T. et al. Mortality at 180-days is affected by serum haptoglobin levels in septic patients with high magnitude serum high mobility group box-1 levels. *Acute Med Surg.* **9**, e726 (2022).
36. Graw, J. A. et al. The role of cell-free hemoglobin and haptoglobin in acute kidney injury in critically ill adults with ARDS and therapy with VV ECMO. *Crit. Care* **26**, 50 (2022).
37. Buehler, P. W., Humar, R. & Schaer, D. J. Haptoglobin Therapeutics and Compartmentalization of Cell-Free Hemoglobin Toxicity. *Trends Mol. Med* **26**, 683–697 (2020).
38. Pirschel, W. et al. Divergent roles of haptoglobin and hemopexin deficiency for disease progression of Shiga-toxin-induced hemolytic-uremic syndrome in mice. *Kidney Int* **101**, 1171–1185 (2022).
39. Raju, S. M. et al. Haptoglobin improves acute phase response and endotoxin tolerance in response to bacterial LPS. *Immunol. Lett.* **207**, 17–27 (2019).
40. Remy, K. E. et al. Haptoglobin improves shock, lung injury, and survival in canine pneumonia. *JCI Insight* **3** (2018).
41. Lai, Z. et al. Disease-Specific haptoglobin N-Glycosylation in inflammatory disorders between cancers and benign diseases of 3 types of female internal genital organs. *Clin. Chim. Acta* **547**, 117420 (2023).
42. Etzerodt, A. & Moestrup, S. K. CD163 and inflammation: biological, diagnostic, and therapeutic aspects. *Antioxid. Redox Signal* **18**, 2352–2363 (2013).
43. Thomsen, J. H., Etzerodt, A., Svendsen, P. & Moestrup, S. K. The haptoglobin-CD163-heme oxygenase-1 pathway for hemoglobin scavenging. *Oxid. Med Cell Longev.* **2013**, 523652 (2013).
44. Philippidis, P. et al. Hemoglobin scavenger receptor CD163 mediates interleukin-10 release and heme oxygenase-1 synthesis: anti-inflammatory monocyte-macrophage responses in vitro, in resolving skin blisters in vivo, and after cardiopulmonary bypass surgery. *Circ. Res* **94**, 119–126 (2004).
45. Sakamoto, A. et al. CD163+ macrophages restrain vascular calcification, promoting the development of high-risk plaque. *JCI Insight* **8** (2023).
46. Ishikawa, E. et al. Direct recognition of the mycobacterial glycolipid, trehalose dimycolate, by C-type lectin Mincle. *J. Exp. Med* **206**, 2879–2888 (2009).
47. Patin, E. C., Orr, S. J. & Schaible, U. E. Macrophage Inducible C-Type Lectin As a Multifunctional Player in Immunity. *Front Immunol.* **8**, 861 (2017).
48. Yamasaki, S. et al. Mincle is an ITAM-coupled activating receptor that senses damaged cells. *Nat. Immunol.* **9**, 1179–1188 (2008).
49. Del Poeta, M., Nimrichter, L., Rodrigues, M. L. & Luberto, C. Synthesis and biological properties of fungal glucosylceramide. *PLoS Pathog.* **10**, e1003832 (2014).
50. Miyake, Y., Ishikawa, E., Ishikawa, T. & Yamasaki, S. Self and nonself recognition through C-type lectin receptor, Mincle. *Self Nonself* **1**, 310–313 (2010).
51. Kirkland, T. N. & Fierer, J. Innate Immune Receptors and Defense Against Primary Pathogenic Fungi. *Vaccines (Basel)* **8**(2020).
52. van Kooyk, Y. & Rabinovich, G. A. Protein-glycan interactions in the control of innate and adaptive immune responses. *Nat. Immunol.* **9**, 593–601 (2008).
53. Haberkamp, C. et al. TNF promotes DECTIN2 family C-type lectin receptor expression in human macrophages. *J. Leukoc. Biol.* **113**, 615–625 (2023).
54. Hatinguais, R., Willment, J. A. & Brown, G. D. C-type lectin receptors in antifungal immunity: Current knowledge and future developments. *Parasite Immunol.* **45**, e12951 (2023).
55. Kong, C., Zhu, Y., Xie, X., Wu, J. & Qian, M. Six potential biomarkers in septic shock: a deep bioinformatics and prospective observational study. *Front Immunol.* **14**, 1184700 (2023).
56. He, D. et al. Single-Cell RNA Sequencing and Transcriptome Analysis Revealed the Immune Microenvironment and Gene Markers of Acute Respiratory Distress Syndrome. *J. Inflamm. Res* **16**, 3205–3217 (2023).
57. Cho, D. S., Schmitt, R. E., Dasgupta, A., Ducharme, A. M. & Doles, J. D. Single-cell deconstruction of post-sepsis skeletal muscle and adipose tissue microenvironments. *J. Cachexia Sarcopenia Muscle* **11**, 1351–1363 (2020).
58. Zhou, W., Zhang, C., Zhuang, Z., Zhang, J. & Zhong, C. Identification of two robust subclasses of sepsis with both prognostic and therapeutic values based on machine learning analysis. *Front Immunol.* **13**, 1040286 (2022).
59. Nakano, M., Saldanha, R., Gobel, A., Kavallaris, M. & Packer, N. H. Identification of glycan structure alterations on cell membrane proteins in desoxypothilone B resistant leukemia cells. *Mol. Cell Proteom.* **10**, M111 009001 (2011).
60. Nakano, M. et al. Bisecting GlcNAc Is a General Suppressor of Terminal Modification of N-glycan. *Mol. Cell Proteom.* **18**, 2044–2057 (2019).
61. Tweedell, R. E., Malireddi, R. K. S. & Kanneganti, T. D. A comprehensive guide to studying inflammasome activation and cell death. *Nat. Protoc.* **15**, 3284–3333 (2020).
62. Kwon, Y. et al. Dimerization of beta(2)-adrenergic receptor is responsible for the constitutive activity subjected to inverse agonism. *Cell Chem. Biol.* **29**, 1532–1540 e1535 (2022).

Acknowledgements

We thank the patients and healthy donors for participating in the study. We thank S.Y. for valuable comments in bioinformatics analysis and helpful discussion. We thank Professor Hong Sung-Tae for providing the pGL4.32[luc2P/NFAT-RE/Hygro] vector for the luciferase assay. We thank H.J.K., S.K., and S.M.J for excellent technical supports. This work was supported by the National Research Foundation of Korea (NRF) grant funded by the Korea government (MSIT) (RS-2023-00255021, RS-2023-00227274 to E.-K.J.; RS-2023-00208127 to S.-Y.P.), by a grant no.2022-08 from the Kangdong Sacred Heart Hospital Fund (to S.Y.P), and by a grant of the Korea Health Technology R&D Project through the Korea Health Industry Development Institute (KHIDI), funded by the Ministry of Health & Welfare, Republic of Korea (RS-2020-KH088690 to S.-Y.P. & E.-K.J.), and by Suh Kyungbae Foundation SUHF-24010035, Samsung Science and Technology Foundation SRFC-MA2402-13 (to S.-Y.P).

Author contributions

E.-K.J., S.-Y.P., S.Y.P., T.R. and S.J. designed the study and wrote the manuscript. S.Y.P., I.S.K., S.-I.L., C.C., and S.-S.J. organized sample acquisition, recruited participants, collected samples and clinical metadata. S.Y.P., I.S.K., C.C., and E.-K.J. analyzed and interpreted clinical data. T.R., S.J., S.Y.P., Y.A., M.N., G.R., H.C., J.C., and T.S. conducted experiments. T.R., C.P., and S.-G.L. performed bioinformatics analysis. S.-Y.P., S.J., Y.A., H.C., M.N., J.C., and E.M. were responsible for Hp isolation and analysis of glycosylation status. Y.J.K., G.K., T.S. and S.Y. performed the animal experiments. E.M., C.P., and S.Y. participated in discussions on content. All authors contributed to the critical review, finalized, and approved the final manuscript. Co-correspondence and request for reprints should be addressed to So Young Park, MD, PhD, sy.park12@gmail.com; Seung-Yeol Park, PhD, seungpark@pos-tech.ac.kr; and Eun-Kyeong Jo, MD, PhD, hayoungj@cnu.ac.kr.

Competing interests

The authors declare no competing interests.

Additional information

Supplementary information The online version contains supplementary material available at <https://doi.org/10.1038/s41467-025-56524-3>.

Correspondence and requests for materials should be addressed to So Young Park, Seung-Yeol Park or Eun-Kyeong Jo.

Peer review information *Nature Communications* thanks Jasmin Knopf, Bernd Lepenies and Hamsa Puthalakath for their contribution to the peer review of this work. A peer review file is available.

Reprints and permissions information is available at <http://www.nature.com/reprints>

Publisher's note Springer Nature remains neutral with regard to jurisdictional claims in published maps and institutional affiliations.

Open Access This article is licensed under a Creative Commons Attribution-NonCommercial-NoDerivatives 4.0 International License, which permits any non-commercial use, sharing, distribution and reproduction in any medium or format, as long as you give appropriate credit to the original author(s) and the source, provide a link to the Creative Commons licence, and indicate if you modified the licensed material. You do not have permission under this licence to share adapted material derived from this article or parts of it. The images or other third party material in this article are included in the article's Creative Commons licence, unless indicated otherwise in a credit line to the material. If material is not included in the article's Creative Commons licence and your intended use is not permitted by statutory regulation or exceeds the permitted use, you will need to obtain permission directly from the copyright holder. To view a copy of this licence, visit <http://creativecommons.org/licenses/by-nc-nd/4.0/>.

© The Author(s) 2025

¹Department of Microbiology, College of Medicine, Chungnam National University, Daejeon, Republic of Korea. ²Department of Medical Science, College of Medicine, Chungnam National University, Daejeon, Republic of Korea. ³Brain Korea 21 FOUR Project for Medical Science, College of Medicine, Chungnam National University, Daejeon, Republic of Korea. ⁴Department of Life Sciences, Pohang University of Science and Technology (POSTECH), Pohang, Republic of Korea. ⁵Division of Pulmonary, Allergy and Critical Care Medicine, Kangdong Sacred Heart Hospital, Seoul, Republic of Korea. ⁶Graduate School of Integrated Sciences for Life, Hiroshima University, Higashi-Hiroshima, Hiroshima, Japan. ⁷Section of Genetics and Physiology, Laboratory of Molecular and Cellular Biology, National Institute of Diabetes and Digestive and Kidney Diseases (NIDDK), National Institutes of Health (NIH), Bethesda, MD, USA. ⁸Department of Pharmacology, College of Medicine, Chungnam National University, Daejeon, Republic of Korea. ⁹Division of Pulmonary and Critical Care Medicine, Department of Internal Medicine, Chungnam National University Hospital, Daejeon, Republic of Korea. ¹⁰Division of Pulmonology and Critical Care Medicine, Department of Internal Medicine, College of Medicine, Chungnam National University, Daejeon, Republic of Korea. ¹¹Department of Molecular Immunology, Research Institute for Microbial Diseases, Osaka University, Suita, Osaka, Japan. ¹²Laboratory of Molecular Immunology, Immunology Frontier Research Center (IFReC), Osaka University, Suita, Osaka, Japan. ¹³Department of Molecular Biochemistry and Clinical Investigation, Osaka University Graduate School of Medicine, Osaka University, Suita, Osaka, Japan. ¹⁴Division of Pulmonary and Critical Care Medicine, Department of Internal Medicine, College of Medicine, Chungnam National University, Daejeon, Republic of Korea. ¹⁵School of Biological Sciences and Technology, Chonnam National University, Gwangju, Republic of Korea. ¹⁶Center for Infectious Disease Education and Research (CiDER), Osaka University, Suita, Osaka, Japan. ¹⁷These authors contributed equally: Taylor Roh, Sungeun Ju, So Young Park. ✉ e-mail: sy.park12@gmail.com; seungpark@postech.ac.kr; hayoungj@cnu.ac.kr